

THIS REPORT HAS BEEN DECLASSIFIED
AND CLEARED FOR PUBLIC RELEASE.

DISTRIBUTION A
APPROVED FOR PUBLIC RELEASE;
DISTRIBUTION UNLIMITED.

Item #
53-12-32641-X

M1-447

MEMORANDUM

206 054

1740

2/25/54

WCOSR
Attn: Mr. Upton

STI
206 054

07740

copy 3/5

**NAVY RESEARCH SECTION
SCIENCE DIVISION
REFERENCE DEPARTMENT
LIBRARY OF CONGRESS**

MAR 11 1952

**FILE COPY
NAVY RESEARCH SECTION
SCIENCE DIVISION
LIBRARY OF CONGRESS
TO BE RETURNED**

TO:
READER CENTER
LIBRARY OF CONGRESS
WASHINGTON, D.C.

17

U. S. NAVAL ORDNANCE TEST STATION

54AA-23392

CONFIDENTIAL

C7740

NOTS TECH. MEMO. No. 129

NOTES ON THE THEORY OF A GYROSCOPIC LEAD
COMPUTING SIGHT OF THE MK 8 TYPE

By

John M. Leffler
Aviation Ordnance Department

WRITTEN: 17 May 1951

PRINTED: 5 July 1951

U. S. NAVAL ORDNANCE TEST STATION
China Lake, California

PRELIMINARY DATA

This material is not to be reproduced and is transmitted for the exclusive use of the indicated recipient. The data presented are tentative and subject to later revision or deletion. The opinions and conclusions expressed herein are those of the individual preparing this report and do not necessarily represent the views of the Naval Ordnance Test Station.

TABLE OF CONTENTS

	<u>Page</u>
INTRODUCTION	1
GENERAL DESCRIPTION OF THE SIGHT UNIT	1
Function of the Sight Unit	1
External Features of the Sight Unit	2
Internal Features of the Sight Unit	2
KINEMATIC LEAD	4
True Kinematic Lead	4
Electromagnetic Constraining Torque	6
Effect of Optical Coupling on the Gyro-Predicted Lead	11
Sensitivity of an Ideal Sight	16
TRAIL OFFSETS	17
MAGNITUDE ERRORS IN THE PREDICTED LEAD	19
Sensitivity of an Actual Sight	19
Offsets of an Actual Sight	46
DIRECTION ERRORS IN THE PREDICTED LEAD	47
Optical Dip	48
Lens Distortion	48
Mechanical Dip	49
Magnetic Dip	50
PRACTICAL ERROR ANALYSIS	51
IMPROVED SIGHTS	52
BIBLIOGRAPHY	55

PRELIMINARY DATA

This material is not to be reproduced and is transmitted for the exclusive use of the indicated recipient. The data presented are tentative and subject to later revision or deletion. The opinions and conclusions expressed herein are those of the individual preparing this report and do not necessarily represent the views of the Naval Ordnance Test Station.

INTRODUCTION

These notes develop the theory of an electromagnetically controlled gyroscopic lead computing sight such as the Sight Unit Mk 8 and discuss its application to the Aircraft Fire Control System Mk 16. After a general description of the sight unit, the theory of the predicted kinematic lead and trail offset is developed. This is followed by an analysis of the errors in magnitude and direction of the predicted lead. After a brief mention of the effect of these errors on the operation of the AFCS Mk 16, suggestions are given for improved design of future sights.

The purpose of this report is to gather together under one cover and present in elementary and non-rigorous fashion some theoretical and experimental facts, which have previously been available only in widely scattered technical reports and memoranda prepared elsewhere, as well as present results of theoretical and experimental work done on the Sight Unit Mk 8 in the Aviation Ordnance Department, Naval Ordnance Test Station, Inyokern, China Lake, California between 1 August 1950 and 31 January 1951. The report is also intended to form a basis for future more quantitative and rigorous investigations of the properties and proper use of the Sight Unit Mk 8 as well as of improved sights.

A rather comprehensive bibliography of published material on the gyroscopic lead computing sight is included.

GENERAL DESCRIPTION OF THE SIGHT UNITFUNCTION OF THE SIGHT UNIT

The function of the sight unit is to present to the pilot a visual indication of the direction in which to fly the aircraft in order to produce the proper lead angle for a hit when forward firing fixed guns and rockets. The sight unit receives four input variables. Three of the inputs are electrical currents, which are generated by a computer. They are the range coil current, the elevation coil current, and the azimuth coil current. The computer determines these currents from its own input variables which are radar range, rocket ballistics, acceleration normal to the wings, angle of attack, angle of skid, air speed, pressure, and temperature. The fourth input variable to the sight unit is the turning rate of the aircraft.

1

PRELIMINARY DATA

This material is not to be reproduced and is transmitted for the exclusive use of the indicated recipient. The data presented are tentative and subject to later revision or deletion. The opinions and conclusions expressed herein are those of the individual preparing this report and do not necessarily represent the views of the Naval Ordnance Test Station.

The fire control system may be thought of as a loop consisting of the pilot, the aircraft, the computer, and the sight unit. There are also independent variables being fed into the computer. The pilot flies the aircraft according to the directions provided by the sight unit, which in turn is controlled by the computer and the motion of the aircraft. The computer inputs are determined partly by the aircraft's motion, which in turn depends on the guidance of the pilot.

EXTERNAL FEATURES OF THE SIGHT UNIT

Externally the sight unit appears as shown in Figure 1 -- an approximately cubical black box on top of which is mounted an inclined glass reflector plate. The sight unit is mounted in the airplane in front of the pilot, who looks through the inclined reflector plate at the target. The pilot also sees the image of a small round source of light. This image is hereafter called the pipper and appears to be located at infinity. The object reticle for this image is located within the sight unit. The rays are rendered parallel by a suitable lens and reflected by the reflector plate into the pilot's eyes.

The position of the pipper is varied in a plane perpendicular to the line of sight by the changing position of a mirror attached to a gyro inside the sight unit. There is also a fixed pipper in the form of a cross, which acts as a fixed reference with respect to which one may estimate the deflection of the gyro pipper.

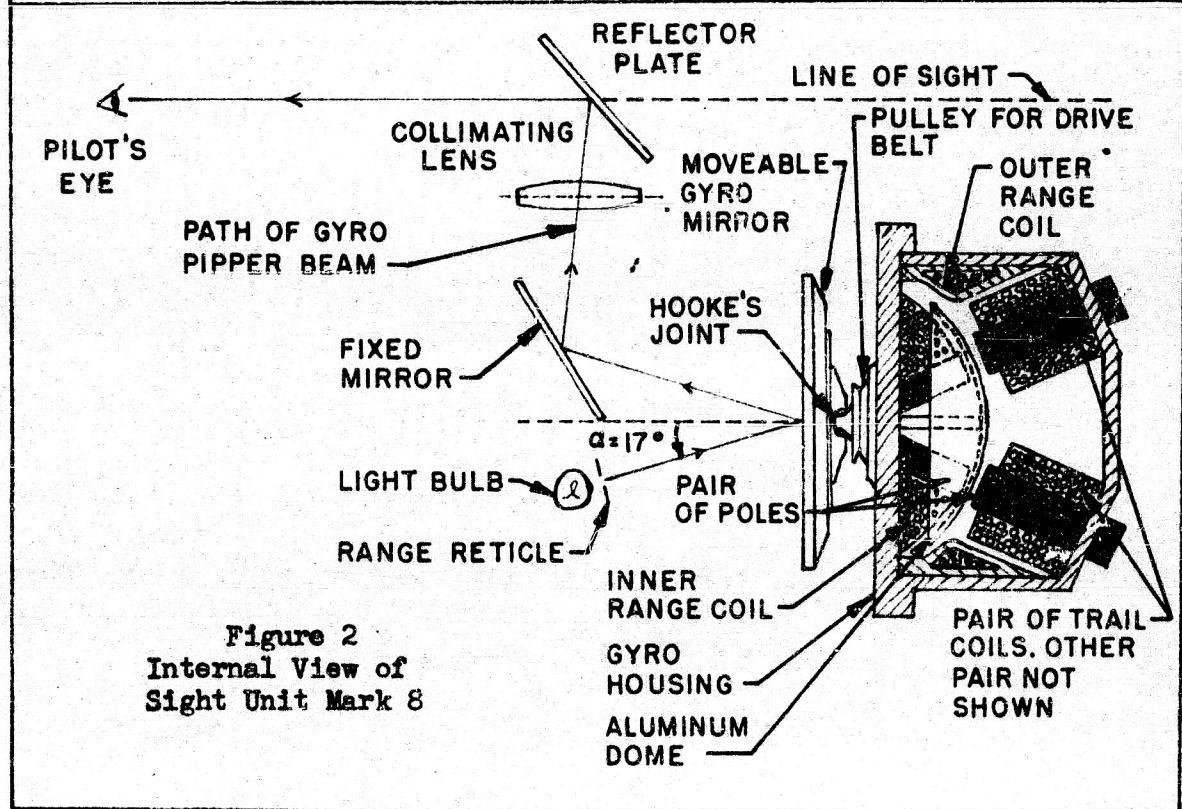
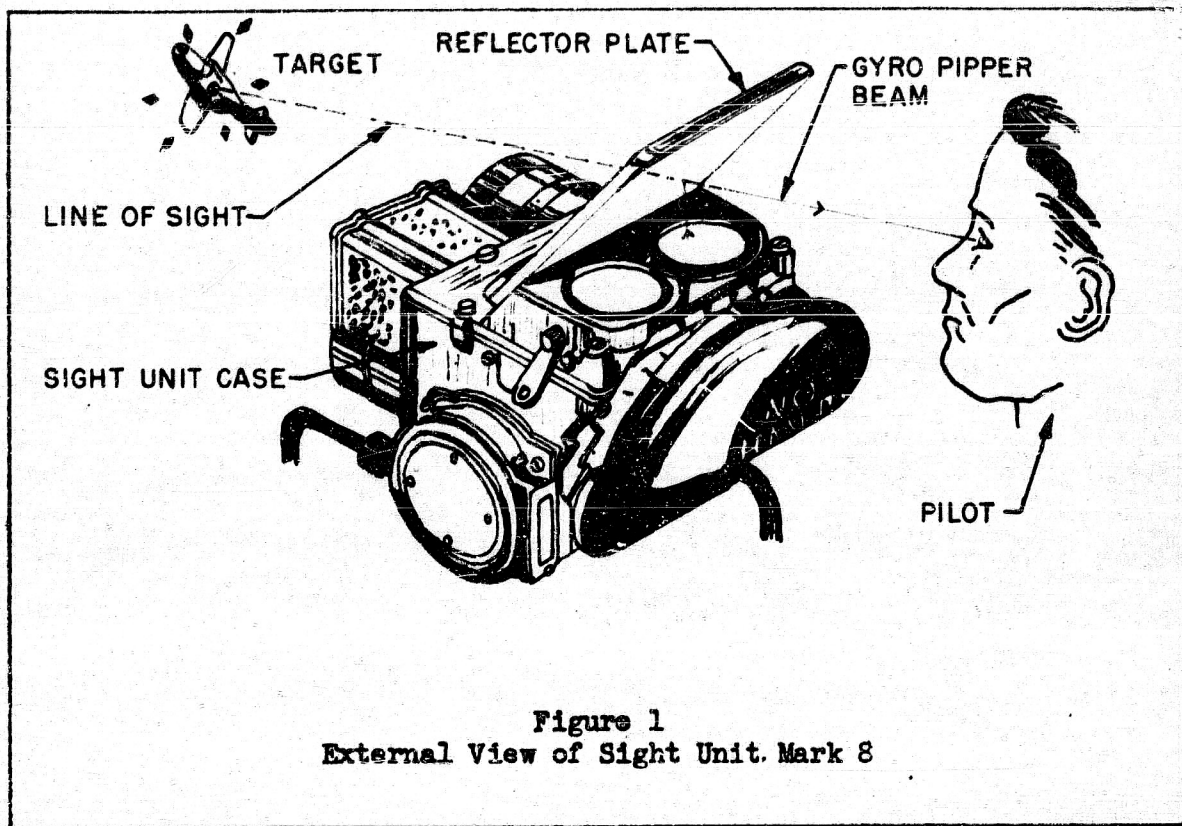
INTERNAL FEATURES OF THE SIGHT UNIT

An internal view of the sight unit is shown in Figure 2. The object which produces the pipper image is formed by a small circular reticle placed in front of a light bulb. Emerging from the reticle, the light beam is reflected first from the mirror attached to the gyro, then from a fixed mirror and finally collimated into parallel rays by a double convex lens.

The movable mirror is attached to one end of and is perpendicular to the rotor of the gyro. A conducting spherical aluminum dome is mounted at the other end of the rotor. The gyro is spun by a drive motor, which applies power, through a spring belt, drive wheel and Hooke's universal joint to the rotor. The Hooke's universal joint allows the spinning gyro to be deflected in both elevation and azimuth.

PRELIMINARY DATA

This material is not to be reproduced and is transmitted for the exclusive use of the indicated recipient. The data presented are tentative and subject to later revision or deletion. The opinions and conclusions expressed herein are those of the individual preparing this report and do not necessarily represent the views of the Naval Ordnance Test Station.



The basic features of a Hooke's joint are presented in Figure 3. Since the Hooke's joint cannot transmit uniform rotation when the gyro axis is inclined to the motor drive shaft, a spring belt drive is provided. The spring belt introduces some rotational play and is designed with the proper length and elastic properties so that the gyro rotor, even though it is not parallel to the motor drive shaft, will have an almost constant angular velocity*.

The dome spins in the air gaps of a magnetic field. Eddy currents induced in the dome produce a drag on it such that the gyro tends to precess toward the effective center of the field. The magnetic field is produced by currents in coils surrounding four pairs of symmetrically placed magnetic poles. The arrangement of the coils and poles is shown in Figures 2 and 4. The range coils encircle all four pairs of poles collectively. The inner and outer range coils are wound in the same direction and produce equal fields in all four air gaps. Thus the line of symmetry of the magnetic fields passes through the geometrical line of symmetry of the array of four pairs of poles.

The gyro may be displaced from the magnetic center line by continuously rotating the sight unit case in space. This is the method by which kinematic lead is predicted as will be explained later. When the effective center line of the magnetic field is rotated in space as a result of rotating the sight unit case, the gyro will attempt to maintain its original position in space. Thus the gyro will lag behind the magnetic center line with a changing magnitude of lag until the restoring torque on the dome is just sufficient to precess the gyro at the angular rate of the case for steady state conditions. This results in the gyro assuming a

* Reference 2 gives the required input angular rate S_1 to be supplied by the drive shaft for a given inclination θ of the gyro axis to obtain an arbitrary constant output angular rate S_0 from the Hooke's joint as

$$S_1 = S_0 \frac{\cos \theta}{1 - \sin^2 S_0 t \sin^2 \theta}$$

PRELIMINARY DATA

This material is not to be reproduced and is transmitted for the exclusive use of the indicated recipient. The data presented are tentative and subject to later revision or deletion. The opinions and conclusions expressed herein are those of the individual preparing this report and do not necessarily represent the views of the Naval Ordnance Test Station.

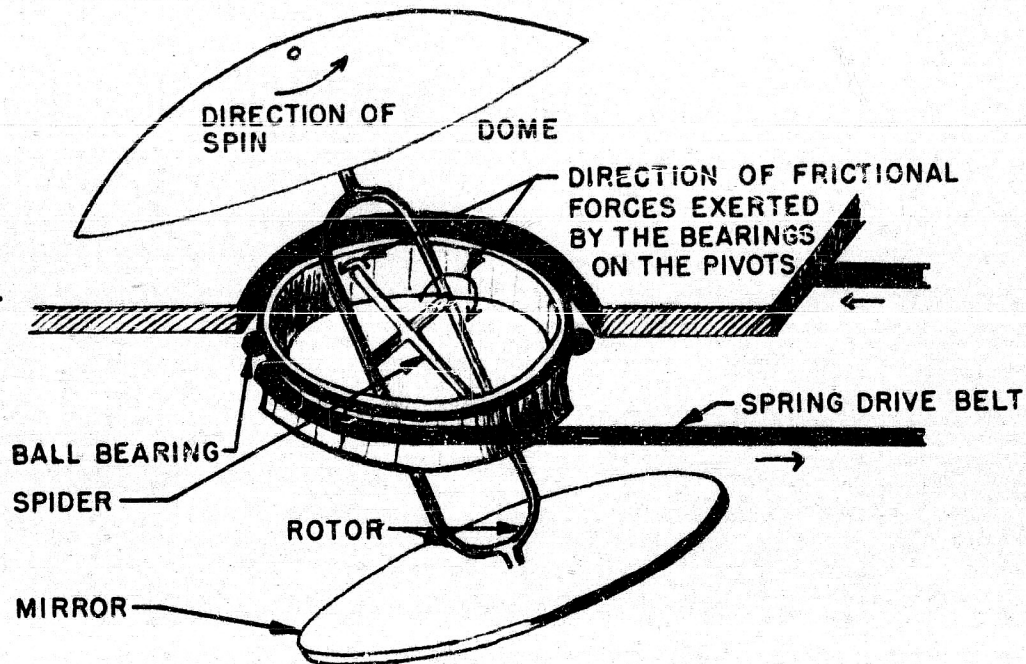


Figure 3
Gyro Assembly and Hooke's Joint

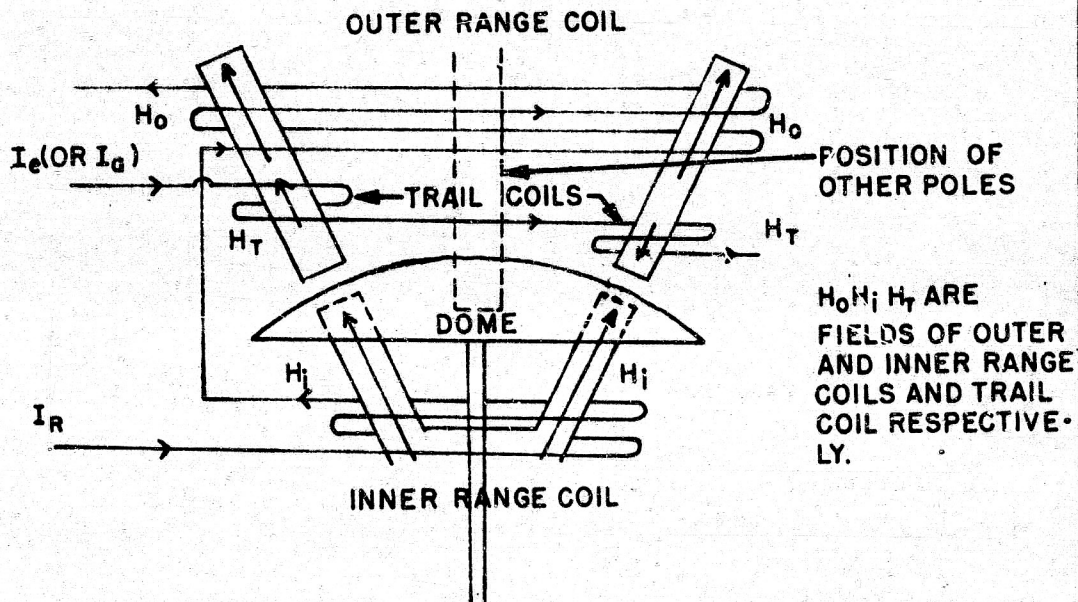


Figure 4
Arrangement of Windings on Pole Pieces

stationary but deflected position with respect to the sight unit case. This deflection gives the mirror and consequently the pipper their deflected positions.

The pipper may also be deflected by changing the position of the magnetic center line with respect to the sight unit case. This is accomplished by energizing the trail coils. The four outer pole pieces are each encircled by an individual coil called a trail coil. The trail coils are connected in series-opposition in vertical and horizontal pairs. Thus current through one pair of trail coils will weaken the field in one air gap but strengthen the field in the opposite air gap by the same amount. This has the effect of shifting the effective center line of the total magnetic field and thus results in a new position of the gyro. One pair of trail coils is used to introduce elevation offsets and the other pair, azimuth offsets. Thus corrections in lead for angle of attack, skid and gravity drop may be introduced as well as any other desired offsets such as the approximately 26 mils contemplated in the Mk 16 Aircraft Fire Control System for the purpose of extending the maximum lead angle in elevation.

KINEMATIC LEAD

TRUE KINEMATIC LEAD

The kinematic lead required by an attacking aircraft when attacking a target is that lead necessary to compensate for the relative motion in space of the attacker and target along their respective flight paths.

The following especially restricted but simple case is considered. Figure 5 shows an attacking aircraft making an attack in the vertical plane on a non-maneuvering target. If the additional components of lead, such as those necessary to compensate for angle of attack, skid and gravity drop are omitted, then the condition for a hit is as shown in the figure. The velocity V_a of the attacking aircraft is shown as lying along the armament datum line (ADL). Also the average velocity V_o of the projectile is shown as lying along the ADL. The lead λ is the angle between the sight line and the ADL. The angle σ of the sight line is taken with respect to a reference line perpendicular to the flight path of the target as is also the angle θ of the ADL. The target velocity is V_T .

4

PRELIMINARY DATA

This material is not to be reproduced and is transmitted for the exclusive use of the indicated recipient. The data presented are tentative and subject to later revision or deletion. The opinions and conclusions expressed herein are those of the individual preparing this report and do not necessarily represent the views of the Naval Ordnance Test Station.

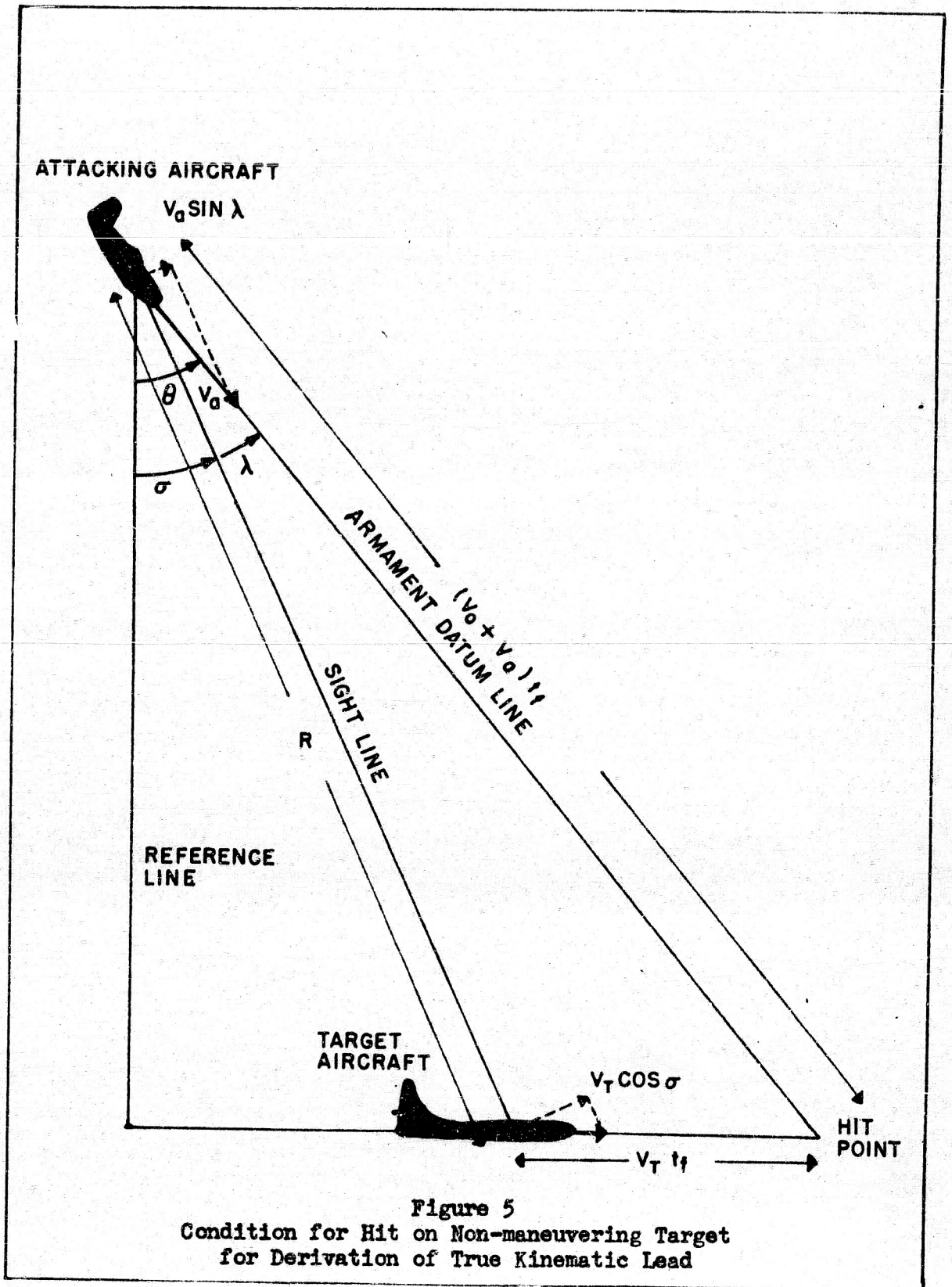


Figure 5
 Condition for Hit on Non-maneuvering Target
 for Derivation of True Kinematic Lead

From the figure

$$\sigma + \lambda = \theta \quad (1)$$

$$\dot{\sigma} + \dot{\lambda} = \dot{\theta} = \omega \quad (2)$$

The law of sines gives

$$\frac{\sin \lambda}{V_T t_f} = \frac{\sin(\pi/2 + \sigma)}{(V_o + V_a) t_f} \quad (3)$$

or

$$V_o \sin \lambda + V_a \sin \lambda = V_T \cos \sigma \quad (4)$$

Due to the rotation of the sight line in space

$$R \dot{\sigma} = V_T \cos \sigma - V_a \sin \lambda \quad (5)$$

Equations (4) and (5) may be combined to obtain

$$\sin \lambda = \frac{R}{V_o} \dot{\sigma} \quad (6)$$

or since λ is usually less than 10 deg,

$$\lambda = \frac{R}{V_o} \dot{\sigma} \quad (7)$$

With the aid of equation (2) the true kinematic lead finally becomes

$$\lambda = \frac{R}{V_o} (\omega - \dot{\lambda}) \quad (8)$$

In the next two sections the expression for the kinematic lead predicted by a gyroscopic sight is developed to allow a comparison with the desired kinematic lead given by equation (8).

PRELIMINARY DATA

This material is not to be reproduced and is transmitted for the exclusive use of the indicated recipient. The data presented are tentative and subject to later revision or deletion. The opinions and conclusions expressed herein are those of the individual preparing this report and do not necessarily represent the views of the Naval Ordnance Test Station.

ELECTROMAGNETIC CONSTRAINING TORQUE

When the dome spins in the air gaps of the magnetic fields, drag forces are developed at each of the four gaps. When the gyro axis is aligned with the magnetic axis, the resultant of the four drag forces on the dome is a couple which tends only to reduce the spin velocity. When the gyro axis is in a deflected position from the magnetic axis, in addition to the spin retarding couple there is a resultant force F_R acting on the dome. This force is shown in Figure 6(a) as acting at the center of the dome and producing a torque $\underline{D} \times F_R$ about the Hooke's joint and a corresponding angular momentum G_R . At any instant the vectorial combination of G_R and the spin angular momentum G_s produces a total angular momentum G . The gyro axis must attempt to line up with G and in so doing precesses toward the magnetic axis. Thus a deflection-constraining effect is produced.

The development of the drag force in a single air gap field will be discussed first. It is necessary to find the functional dependence of this force on gyro deflection, magnetic field, conductivity of the dome and other factors. Referring to Figure 6(b) it is possible to analyze the effect of the magnetic field on the spinning dome. The dome is spinning with an angular velocity S , which corresponds to a tangential velocity

$$v = SD \sin \phi \quad (9)$$

at a point P of colatitude ϕ in the presence of the magnetic induction \underline{B} . Conduction electrons of charge e in the vicinity of point P feel a force

$$\underline{F}_e = -e\underline{v} \times \underline{B} \quad (10)$$

or an electric field

$$\underline{E} = \frac{\underline{F}_e}{e} = -\underline{v} \times \underline{B} \quad (11)$$

The field is in such a direction as to urge electrons toward the axis of the dome or positive current toward the edge of the dome. An approximate mapping of the eddy current flow is shown in Figure 6(c).

PRELIMINARY DATA

This material is not to be reproduced and is transmitted for the exclusive use of the indicated recipient. The data presented are tentative and subject to later revision or deletion. The opinions and conclusions expressed herein are those of the individual preparing this report and do not necessarily represent the views of the Naval Ordnance Test Station.

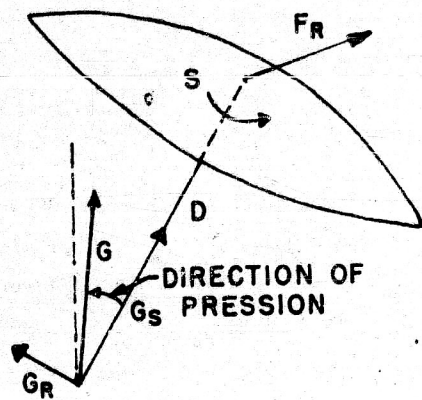


Figure 6(a)
Precession of Gyro Axis

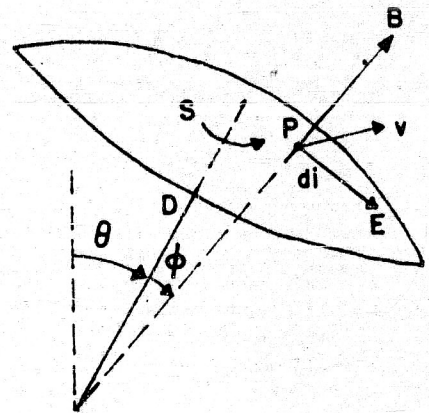


Figure 6(b)
Production of Eddy Current
di along E

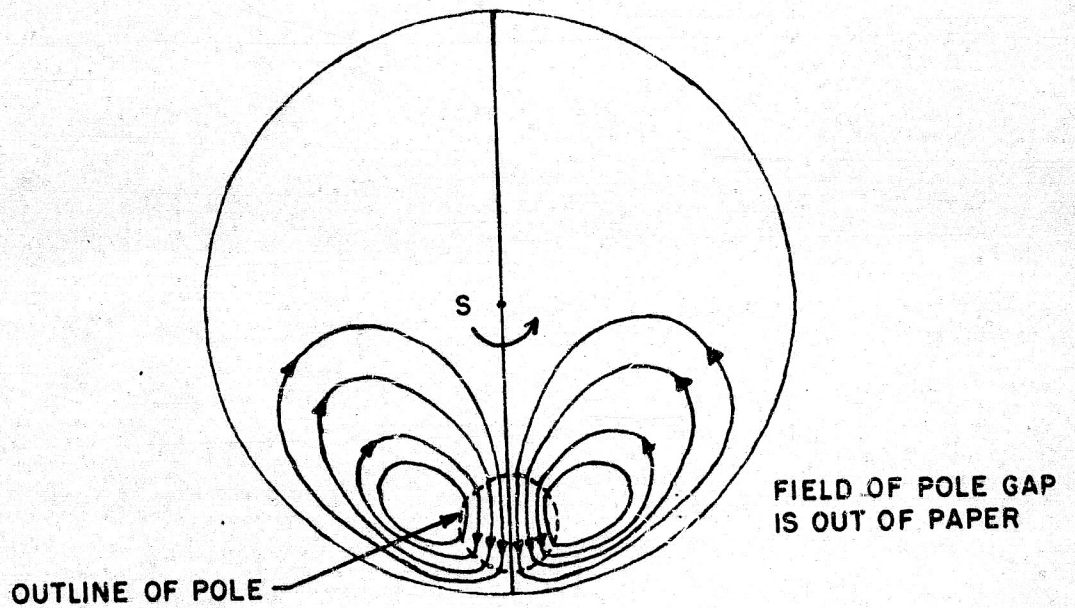


Figure 6(c)
Eddy Current Pattern on Spinning Dome for Single Pair of Poles

A positive current element $d\mathbf{i}$ in the presence of \mathbf{B} feels a force

$$d\mathbf{F} = d\mathbf{i} \times \mathbf{B} \quad (12)$$

If \mathbf{j} is the current density and dV is a volume element of the dome at point P, then

$$d\mathbf{i} = \mathbf{j} dV \quad (13)$$

or

$$d\mathbf{F} = \mathbf{j} dV \times \mathbf{B} \quad (14)$$

By Ohm's law

$$\mathbf{j} = \sigma \mathbf{E} = \sigma \mathbf{v} \times \mathbf{B} \quad (15)$$

where σ is the conductivity of the dome. Therefore, dropping the vector notation,

$$dF = \sigma v B^2 dV \quad (16)$$

Since the dome is not ferromagnetic, the relation

$$\mathbf{B} = \mu \mathbf{H} \quad (17)$$

may be used with a constant value of the permeability.

Consequently

$$dF = \sigma \mu^2 H^2 v dV \quad (18)$$

After substituting equation (9) into equation (18)

$$dF = \sigma \mu^2 H^2 S D \sin \phi dV \quad (19)$$

it is assumed that the magnetic field is appreciable only under the pole piece. Then the integrated force over the small volume V of

PRELIMINARY DATA

This material is not to be reproduced and is transmitted for the exclusive use of the indicated recipient. The data presented are tentative and subject to later revision or deletion. The opinions and conclusions expressed herein are those of the individual preparing this report and do not necessarily represent the views of the Naval Ordnance Test Station.

the dome immediately under a pole piece is

$$F = \sigma \mu^2 H^2 S D \overline{\sin \phi} V \quad (20)$$

where $\overline{\sin \phi}$ is an average value taken over the volume. Since V is small, the approximation $\overline{\sin \phi} \approx \sin \phi$ is used hereafter unless otherwise specified. If ϵ is the thickness of the dome and A is the area of the pole face, then the fundamental equation for the drag force at a single air gap is

$$F = \sigma \mu^2 H^2 S D \epsilon A \sin \phi \quad (21)$$

Equation (21) may now be used to calculate the force at each of the four pole gaps. For the following analysis it is profitable to let

$$c = \sigma \mu^2 S D \epsilon A \quad (22)$$

so that

$$F = c H^2 \sin \phi \quad (23)$$

In general, when trail coil currents are present and the angular rate of the sight unit is in some arbitrary direction, the four fields will be different and result in four difference forces

$$\left. \begin{aligned} F_1 &= c H_1^2 \sin \phi_1 \\ F_2 &= c H_2^2 \sin \phi_2 \\ F_3 &= c H_3^2 \sin \phi_3 \\ F_4 &= c H_4^2 \sin \phi_4 \end{aligned} \right\} \quad (24)$$

For simplicity and retention of the physical picture the present derivation of the gyro's equation of motion is rather qualitative and restricted in scope. Consideration is given to the special case of a gyro deflection in azimuth only. The gyro is under the influence of an angular rotation of the sight unit case in the azimuth plane and an azimuth trail offset as shown in Figure 7. The more rigorous and more complete equations for the general case of an

PRELIMINARY DATA

This material is not to be reproduced and is transmitted for the exclusive use of the indicated recipient. The data presented are tentative and subject to later revision or deletion. The opinions and conclusions expressed herein are those of the individual preparing this report and do not necessarily represent the views of the Naval Ordnance Test Station.

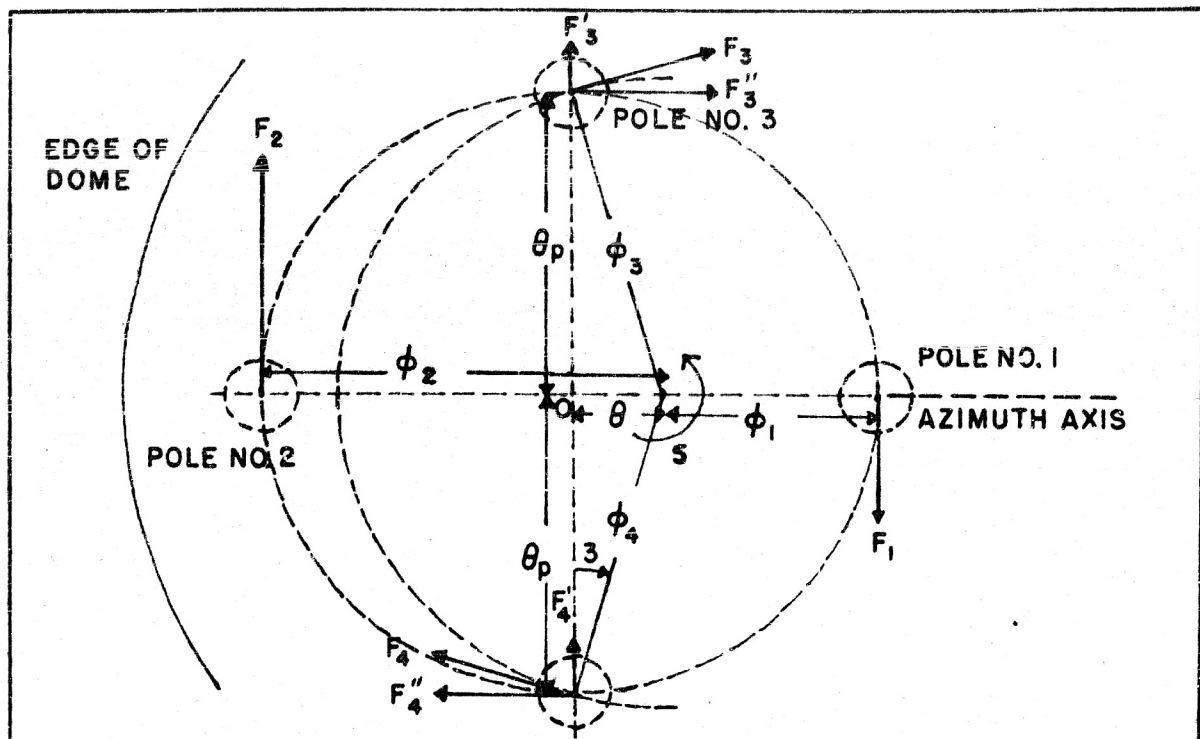


Figure 7(a)
Top View of Dome with Eddy Current Forces for a Deflection in Azimuth

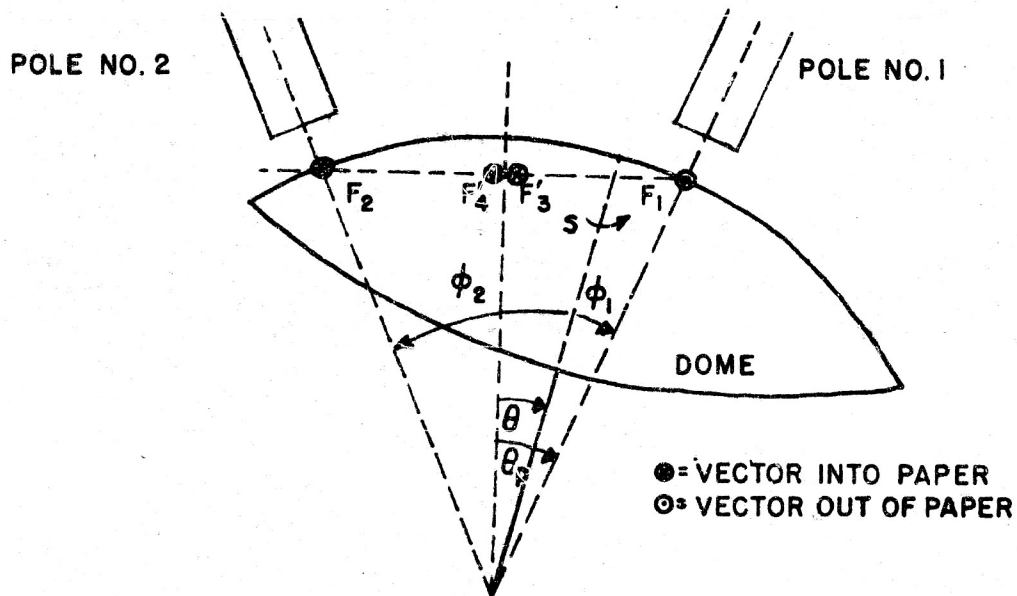


Figure 7(b)
Side View of Dome with Eddy Current Forces for a Deflection in Azimuth

arbitrary plane of rotation in the presence of both elevation and azimuth effects are given and interpreted in later sections of this report.

Making use of the angular relations in Figure 7 and spherical trigonometry, one obtains

$$\left. \begin{aligned} \sin \phi_1 &= \sin(\theta_p - \theta) \\ \sin \phi_2 &= \sin(\theta_p + \theta) \\ \sin \phi_3 &= \sin \phi_4 = \cos \sqrt{\sin^2 \theta_p + \tan^2 \theta} \end{aligned} \right\} \quad (25)$$

The precessing torque is obtained from the resultant of the forces acting perpendicular to the gyro deflection. These forces are

$$\left. \begin{aligned} F_1 &= cH_1^2 \sin(\theta_p - \theta) \\ F_2 &= cH_2^2 \sin(\theta_p + \theta) \\ F_3' &= F_3 \sin \gamma = cH_3^2 \sin \theta \\ F_4' &= F_4 \sin \gamma = cH_4^2 \sin \theta \end{aligned} \right\} \quad (26)$$

where

$$\sin \gamma = \frac{\tan \theta}{\sqrt{\sin^2 \theta_p + \tan^2 \theta}} \quad (27)$$

By conservation of moments it may be shown that the pair of forces F_1 and F_2 may be replaced by a single force $F_2 - F_1$ acting at the center of the dome and a couple of magnitude $(F_1 + F_2)D \sin \theta_p + (F_2 - F_1)D \sin \theta$ which opposes the spin. Similarly the forces F_3' and F_4' may be replaced by a single force $F_3' + F_4'$ acting at the center of the dome and a couple of magnitude $(F_3' + F_4')D \sin \theta$. There is an additional spin-retarding couple of magnitude $F_3'D \sin \theta_p$ produced by the components of F_3 and F_4 which are parallel to the deflection.

Thus the resultant total force acting at the center of the dome is

$$F_R = F_2 - F_1 + F_3' + F_4' \quad (28)$$

PRELIMINARY DATA

This material is not to be reproduced and is transmitted for the exclusive use of the indicated recipient. The data presented are tentative and subject to later revision or deletion. The opinions and conclusions expressed herein are those of the individual preparing this report and do not necessarily represent the views of the Naval Ordnance Test Station.

and the total spin-retarding couple is

$$\begin{aligned} M_c = & (F_1 + F_2)D \sin \theta_p + (F_2 - F_1)D \sin \theta \\ & + (F_3' + F_4')D \sin \theta + F_3 D \sin \theta_p \end{aligned} \quad (29)$$

By multiplying the total force by its lever arm D the eddy current precessing torque T_E is obtained as

$$T_E = D \times F_R = Dc [H_2^2 \sin(\theta_p + \theta) - H_1^2 \sin(\theta_p - \theta) + (H_3^2 + H_4^2) \sin \theta] \quad (30)$$

In the present case there are currents present in the azimuth trail coils as well as in the range coil so that

$$\left. \begin{aligned} H_1 &= H_R + H_a \\ H_2 &= H_R - H_a \\ H_3 &= H_R \\ H_4 &= H_R \end{aligned} \right\} \quad (31)$$

where H_R is the field due to the range coil current, H_a is due to the azimuth coil current. Substitution of equations (31) into equation (30) and expansion of the trigonometric functions yields

$$T_E = 2Dc \left\{ [H_R^2(1 + \cos \theta_p) + H_a^2 \cos \theta_p] \sin \theta - 2H_R H_a \sin \theta_p \right\} \quad (32)$$

Applying Newton's second law of motion for angular rotation in the plane of the deflection of the gyro axis one has

$$M S \ddot{\eta} = T_E \quad (33)$$

where M is the moment of inertia about the gyro axis and $\ddot{\eta}$ is the precessional angular velocity in the plane of the deflection. When a constant turning rate ω is impressed upon the sight unit case the gyro will deflect until the torque T_E is sufficient to precess the

gyro at the same velocity (i.e., $\dot{\eta} = \omega$). Therefore from equations (33) and (32) the steady state equation of motion becomes

$$MS\omega = 2Dc \left\{ \left[H_R^2(1 + \cos \theta_p) + H_c^2 \cos \theta_p \right] \sin \theta - 2H_R H_a \sin \theta_p \cos \theta \right\} \quad (34)$$

Since the gyro deflection θ will always be under 14 degrees, the small angle approximations of $\sin \theta \approx \theta$ and $\cos \theta \approx 1$, as well as $\cos \theta_p \approx 1$, $\cos \theta_p = \cos 23.5^\circ \approx 1$ may be used with no more than 1 per cent error in $\sin \theta$ and 3 per cent in $\cos \theta$. The gyro deflection then becomes

$$\theta = \frac{MS}{2DcH_R^2 \left(2 + \frac{H_a^2}{H_R^2} \right)} \omega + \frac{2\theta_p \frac{H_a}{H_R}}{2 + \frac{H_a^2}{H_R^2}} \quad (35)$$

Further interpretation and application of the above equation to obtain the predicted lead must await an analysis of the connection between the gyro deflection and the pipper deflection (or sight line deflection when properly tracking). This connection will be given in the following section.

EFFECT OF OPTICAL COUPLING ON THE GYRO-PREDICTED LEAD

After a brief examination of the path of the pipper beam as shown in Figure 2, it will be apparent that the sight line will not deflect through the same angles as the gyro axis but rather will deflect through angles which are proportional to the gyro deflections.

To derive the relation between the gyro and the line of sight deflections it is necessary to consider the geometrical optics of the sight. A simplified diagram of the path of the pipper beam is shown in Figure 8. The fixed mirror has been removed, and the point C indicates the optical position of the lens. In order to insure parallel rays emerging from the sight unit, the object reticle R is placed at the focal point of the lens. Thus the total distance traveled by the beam from reticle to lens is f , the focal length. The distance from the reticle to the gyro mirror is d .

PRELIMINARY DATA

This material is not to be reproduced and is transmitted for the exclusive use of the indicated recipient. The data presented are tentative and subject to later revision or deletion. The opinions and conclusions expressed herein are those of the individual preparing this report and do not necessarily represent the views of the Naval Ordnance Test Station.

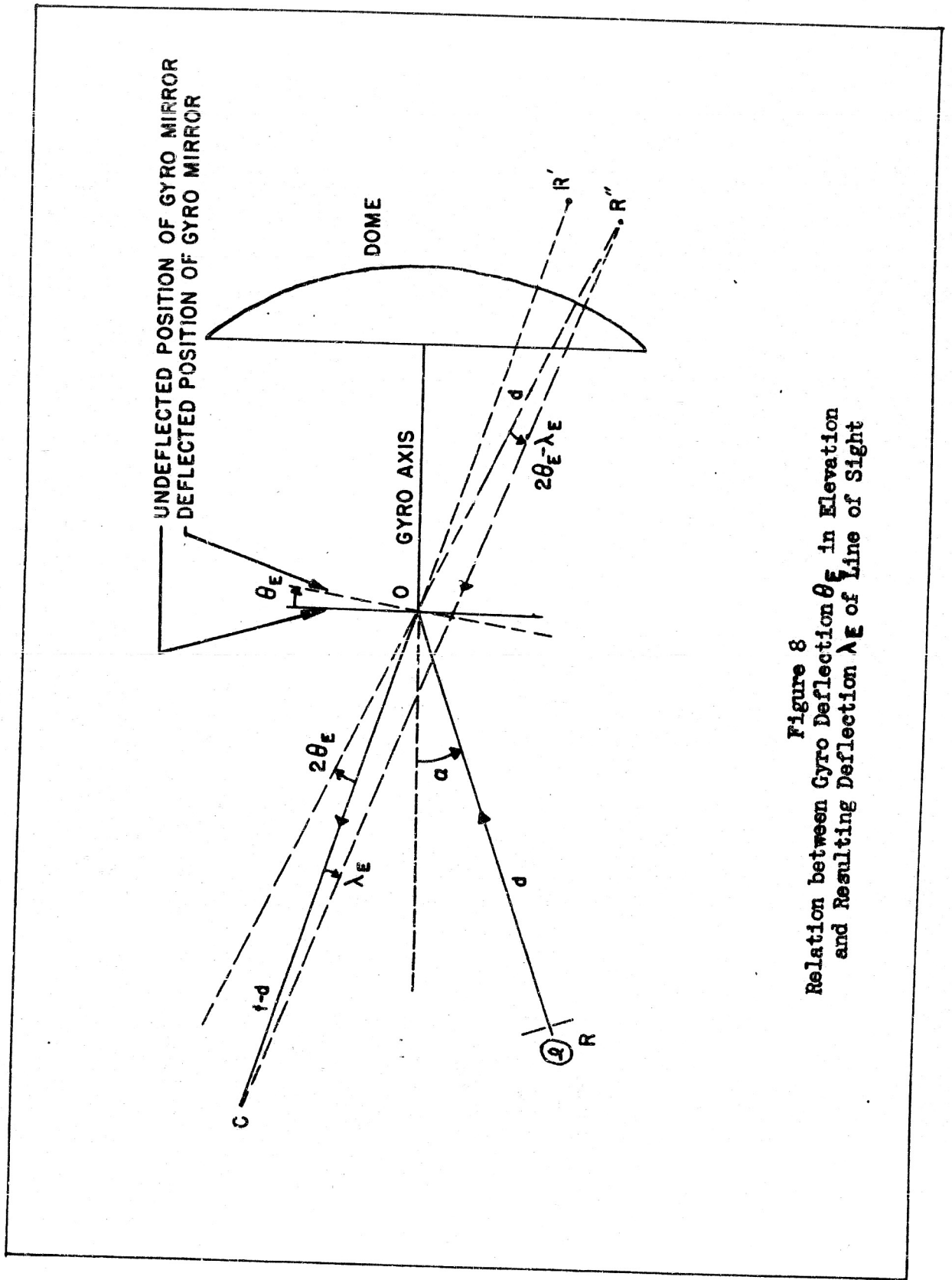


Figure 8
 Relation between Gyro Deflection θ_E in Elevation
 and Resulting Deflection λ_E of Line of Sight

For simplicity the present analysis is two dimensional and concerned with a deflection of the gyro mirror in elevation only. The analysis of the deflection in azimuth only proceeds along similar lines. The three dimensional analysis for both an elevation and an azimuth deflection is considerably more complicated, and for the derivation the reader is referred to References 8, 9, and 10.

Returning to Figure 8 it is apparent that from the lens position at C the undeflected image of the pipper will appear to be at R'. The line of sight will appear to be along R'C. When the gyro mirror is deflected through an angle θ_E , the reflected beam will change direction by an angle $2\theta_E$. Again from point C the deflected pipper image will appear to be at R'', and the line of sight will appear to be along R''C. Thus the deflection of the line of sight is

From the law of sines

$$\frac{\sin \lambda_E}{d} = \frac{\sin(2\theta_E - \lambda_E)}{f - d} \quad (36)$$

The angles λ_E and θ_E are small and therefore the small angle approximation gives

$$\frac{\lambda_E}{d} = \frac{2\theta_E - \lambda_E}{f - d} \quad (37)$$

or

$$\lambda_E = \frac{2d}{f} \theta_E \quad (38)$$

Since $f > 2d$, it is apparent that the deflection of the line of sight is always less than the gyro deflection. The difference between the gyro and sight line deflections is

$$\theta_E - \lambda_E = \frac{f}{2d} \lambda_E - \lambda_E = \left(\frac{f}{2d} - 1 \right) \lambda_E \quad (39)$$

It is convenient to express the factor $f/2d - 1$ as a positive constant a . Finally one obtains

$$\lambda_E = \frac{\theta_E}{1 + a} \quad (40)$$

PRELIMINARY DATA

12

This material is not to be reproduced and is transmitted for the exclusive use of the indicated recipient. The data presented are tentative and subject to later revision or deletion. The opinions and conclusions expressed herein are those of the individual preparing this report and do not necessarily represent the views of the Naval Ordnance Test Station.

The similar result of the analysis for azimuth deflection only is

$$\lambda_A = \frac{2d \cos \alpha}{f} \theta_A \quad (41)$$

where θ_A is the deflection of the gyro mirror in azimuth and α is the angle between the normal to the gyro mirror in the undeflected position and the incident beam RO. For small α , $\cos \alpha \approx 1$, which results in almost identical coupling in azimuth and elevation. The actual value of α of 17 deg for the Sight Unit Mk 8 results in a 4.3 per cent difference of the proportionality constant for coupling in azimuth from that for coupling in elevation. In the Sight Unit Mk 11 this error is halved. (See Reference 19.)

If the constant of proportionality between λ and θ is to remain of the form $1/(1+a)$ for all directions of deflection from elevation to azimuth, then it is apparent that the value of "a" is different for each different direction of deflection. It is shown in reference 11 that

$$a_{\beta_v} = \frac{f}{2d} \sqrt{\frac{1 + \tan^2 \beta_v}{\cos^2 \alpha \tan^2 \beta_v + 1}} \quad (42)$$

where a_{β_v} is the "a" value when the azimuth axis of the sight is inclined at an angle β_v with respect to the horizontal plane and the piper is deflected vertically by rotation of the sight in the vertical plane.

In the sight unit calibration work (see reference 10 and 12) at the Naval Ordnance Plant, Indianapolis, (NOPI), the intermediate "a" value was chosen for the tactically frequent condition of $\beta_v = 30$ deg where the attack is in the vertical plane, for which equation (42) gives 0.431. In more recent calibration work (see references 11 and 13) at NOTS, an "a" value was chosen as 0.439 which corresponds to a bank angle of 38 deg for an attack in the vertical plane and represents an average constant between the tactical extremes of an attack in the vertical plane with no bank angle and an attack in the horizontal plane with a 30 deg bank angle.

Further discussion of the effect of the variation of optical coupling with direction of deflection will be given in the sections

PRELIMINARY DATA

This material is not to be reproduced and is transmitted for the exclusive use of the indicated recipient. The data presented are tentative and subject to later revision or deletion. The opinions and conclusions expressed herein are those of the individual preparing this report and do not necessarily represent the views of the Naval Ordnance Test Station.

on errors in the predicted lead.

Application of the optical coupling factor to the gyro deflection in equation (35) gives the gyro-predicted lead as

$$\lambda_G = \frac{MS}{2DcH_R^2(1+a)} \omega + \frac{2\theta_p}{(1+a)} \frac{H_a}{H_R} \frac{1}{\left(2 + \frac{H_a^2}{H_R^2}\right)} \quad (43)$$

The first term on the right hand side of equation (43) is the kinematic lead and the second term is the azimuth offset, which will be discussed later.

In the absence of the trail offset the kinematic lead becomes

$$\lambda_G = \frac{MS}{4DcH_R^2(1+a)} \omega \quad (44)$$

Recalling from equation (22) that C contains the spin velocity S it is apparent that the lead is independent of S or

$$\lambda_G = \frac{M}{40\pi^2 \epsilon ADH_R^2(1+a)} \omega \quad (45)$$

The magnetic field H_R is proportional to the range coil current I_R so that

$$H_R = (K_1N_1 + K_2N_2)I_R \quad (46)$$

K_1 and K_2 are form factors and N_1 and N_2 are the numbers of turns on the inner and outer range coils, respectively. Thus upon consolidating the constant factors by the substitution

$$K^2 = \frac{M}{40\pi^2 \epsilon AD(K_1N_1 + K_2N_2)} \quad (47)$$

PRELIMINARY DATA

This material is not to be reproduced and is transmitted for the exclusive use of the indicated recipient. The data presented are tentative and subject to later revision or deletion. The opinions and conclusions expressed herein are those of the individual preparing this report and do not necessarily represent the views of the Naval Ordnance Test Station.

the gyro-predicted lead finally becomes

$$\lambda_G = \frac{K^2}{(1+a)I_R^2} \omega \quad (48)$$

The above equation (48) is used to define the sight sensitivity in the next section.

A comparison of the true kinematic of equation (8) lead and the gyro-predicted lead may be made with the aid of Figure 9. Returning to Newton's law of motion for the sight as given in equation (33) and expressing the constraining torque T_E as

$$T_E = \frac{MS I_R^2}{K^2} \ddot{\theta} = \frac{MS I_R^2}{K^2} (1+a) \dot{\lambda}_G \quad (49)$$

one obtains the precession rate as

$$\dot{\eta} = \frac{I_R^2 (1+a) \dot{\lambda}_G}{K^2} \quad (50)$$

From Figure 9 the angle of the gyro axis referred to the reference line, which is perpendicular to the straight and level flight path of the target is

$$\eta = \sigma - a \lambda_G \quad (51)$$

The precession velocity becomes

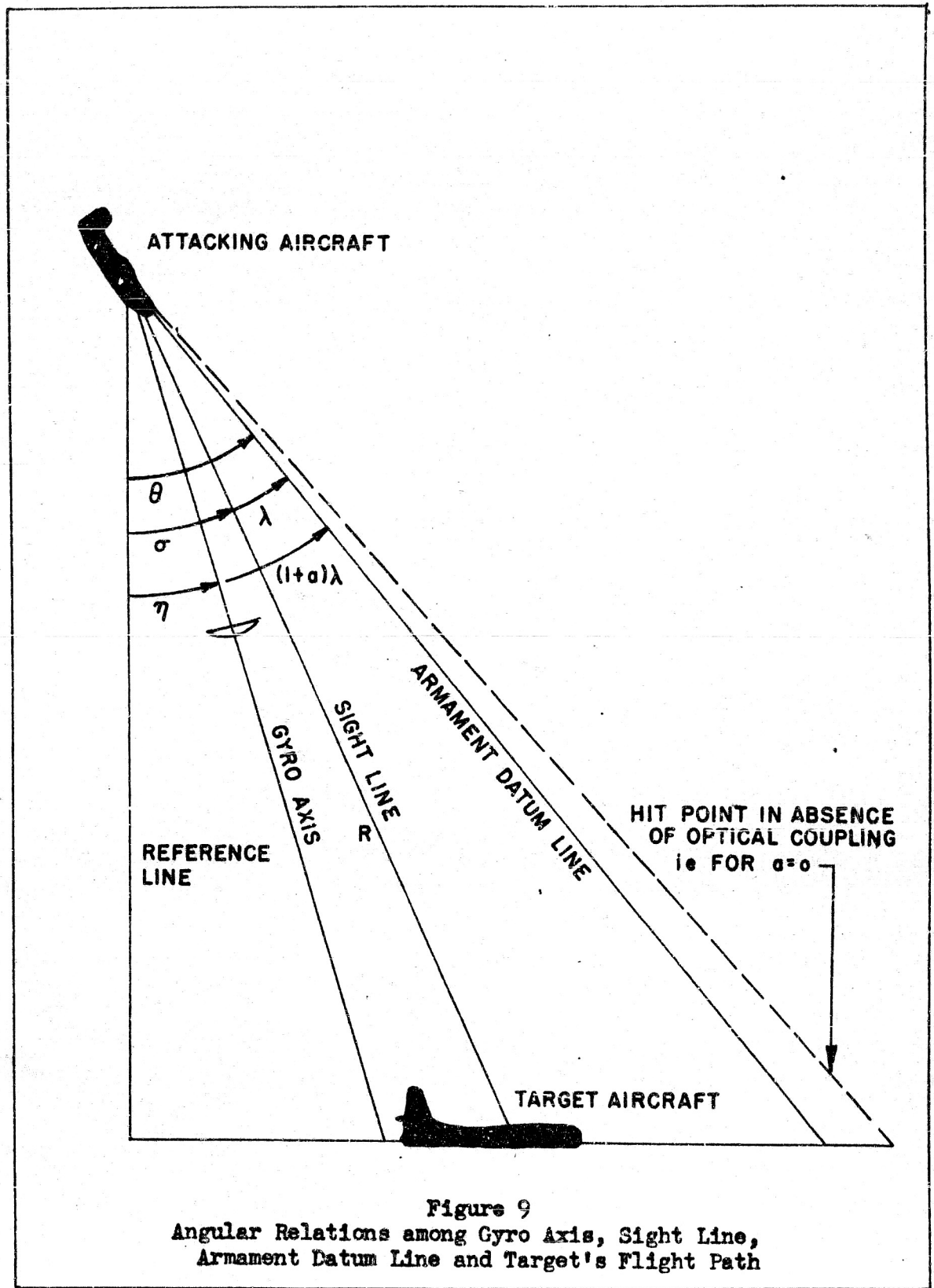
$$\dot{\eta} = \dot{\sigma} - a \dot{\lambda}_G \quad (52)$$

and when it is substituted into equation (5) the gyro-predicted lead becomes

$$\lambda_G = \frac{K^2}{(1+a)I_R^2} \dot{\sigma} - \frac{a}{(1+a)} \frac{K^2}{I_R^2} \dot{\lambda}_G \quad (53)$$

PRELIMINARY DATA

This material is not to be reproduced and is transmitted for the exclusive use of the indicated recipient. The data presented are tentative and subject to later revision or deletion. The opinions and conclusions expressed herein are those of the individual preparing this report and do not necessarily represent the views of the Naval Ordnance Test Station.



Replacing the rate of the sight line by $\dot{\sigma} = \omega - \dot{\lambda}_G$ gives

$$\lambda_G = \frac{K^2}{I_R^2} \left(\frac{\omega}{1+a} - \dot{\lambda}_G \right) \quad (54)$$

Comparison of $\dot{\lambda}_G$ with the true kinematic lead $\dot{\lambda}$ is made possible by employing the AFCS Mk 16 computer-mechanized relation

$$\frac{K^2}{I_R^2} = \frac{R}{V_0} \quad (55)$$

Then the gyro-predicted lead becomes

$$\lambda_G = \frac{R}{V_0} \left(\frac{\omega}{1+a} - \dot{\lambda}_G \right) \quad (56)$$

A comparison of equations (8) and (56) shows that due to the presence of the $1+a$ factor the sight predicts a lead which is smaller than the true value. In the expression for the total lead predicted by the AFCS Mk 16 other terms are added to equation (56) so that this reduction is partially compensated. For more details on this compensation the reader is referred to reference 4.

SENSITIVITY OF AN IDEAL SIGHT

The proportionality constant between the gyro-predicted lead λ_G and the turning rate of the sight line, which for the steady state (i.e., $\dot{\lambda}_G = 0$) is the turning rate ω of the aircraft, is defined as the sensitivity

$$\mu = \frac{\lambda_G}{\omega} \quad (57)$$

From equations (56) and (48) it follows that

$$\mu = \frac{R}{(1+a)V_0} \quad (58)$$

PRELIMINARY DATA

This material is not to be reproduced and is transmitted for the exclusive use of the indicated recipient. The data presented are tentative and subject to later revision or deletion. The opinions and conclusions expressed herein are those of the individual preparing this report and do not necessarily represent the views of the Naval Ordnance Test Station.

and also

$$\mu = \frac{K^2}{(1 + a)I_R^2} \quad (59)$$

If K and a are assumed to be constant, then equation (59) gives the sensitivity of the ideal sight wherein there is no dependence of μ upon a . A plot of sensitivity for the ideal sight versus turning rate of the aircraft would appear as in Figure 10. Thus as the range coil current is decreased, the sensitivity of the sight is increased. It is to be noted that the sensitivity has the units of time and is usually given in seconds.

For calibration purposes the computer mechanization constant to be used in equation (55) can be determined for the ideal sight by a single application of the formula

$$K = I_R \sqrt{(1 + a) \frac{\lambda_G}{\omega}} \quad (60)$$

which is obtained from combining equations (57) and (59). The sight can be placed on a rate table, which simulates the constant rate ω of the aircraft. I_R is applied to the range coil, and the resulting lead λ_G is read. However, the calibration of an actual sight cannot be reliably based on one such measurement. The behavior of an actual sight whose sensitivity μ does depend upon the aircraft turning rate ω is discussed in a later section.

TRAIL OFFSETS

When the trail coils are energized as well as the range coils, the gyro axis assumes a deflected position even in the absence of an angular rate of the aircraft. This deflected position determines the trail offset. As was previously pointed out in connection with the equation (43), the second term is the azimuth offset

$$\lambda_a = \frac{2 \theta_p}{(1 + a)} \frac{H_a}{H_R} \frac{1}{\left(2 + \frac{H_a^2}{H_R^2}\right)} \quad (61)$$

PRELIMINARY DATA

This material is not to be reproduced and is transmitted for the exclusive use of the indicated recipient. The data presented are tentative and subject to later revision or deletion. The opinions and conclusions expressed herein are those of the individual preparing this report and do not necessarily represent the views of the Naval Ordnance Test Station.

The sight was intended to be used in the region where the ratios H_a/H_R and H_e/H_R are small so that the squared terms may be neglected for summary. The effect of neglecting the squared term is discussed later in connection with the trail offsets of an actual sight. The azimuth trail offset for an ideal sight is

$$\lambda_a = \frac{\theta_p}{1+a} \frac{H_a}{H_R} \quad (62)$$

Introducing the numbers of turns and form factors as was done in equation (46) and also letting

$$H_a = K_a N_a I_a \quad (63)$$

one obtains

$$\lambda_a = \frac{\theta_p K_a N_a I_a}{(1+a)(K_1 N_1 + K_2 N_2) I_R} \quad (64)$$

By letting the azimuth trail calibration constant

$$k_a = \frac{\theta_p K_a N_a}{(1+a)(K_1 N_1 + K_2 N_2)} \quad (65)$$

one finally obtains for the ideal azimuth trail offset

$$\lambda_a = k_a \frac{I_a}{I_R} \quad (66)$$

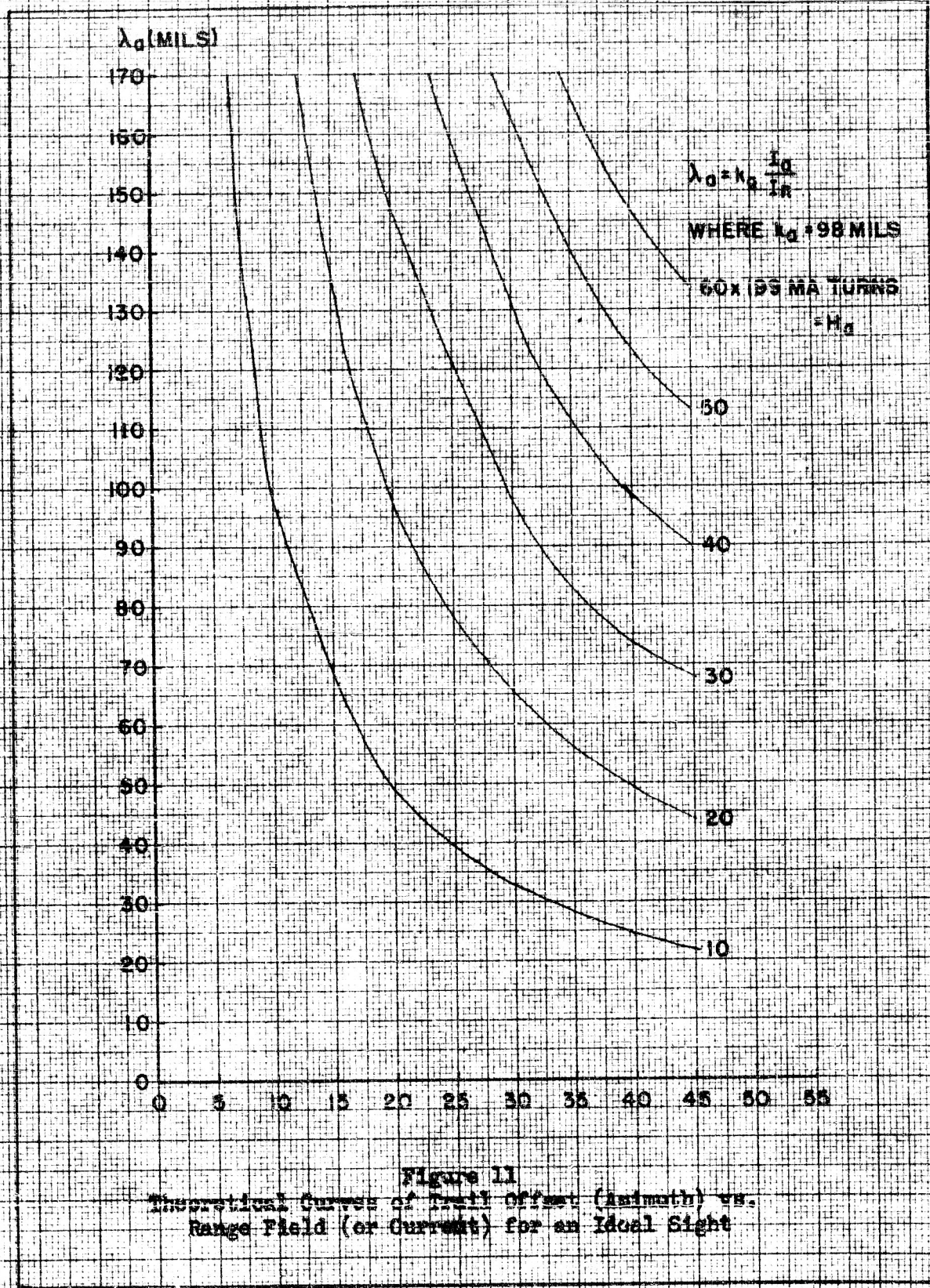
A similar relation is obtained for the elevation offset. Thus

$$\lambda_e = k_e \frac{I_e}{I_R} \quad (67)$$

A set of curves showing this ideal hyperbolic dependence of trail offset on range coil current for different trail coil currents is given in Figure 11.

PRELIMINARY DATA

This material is not to be reproduced and is transmitted for the exclusive use of the indicated recipient. The data presented are tentative and subject to later revision or deletion. The opinions and conclusions expressed herein are those of the individual preparing this report and do not necessarily represent the views of the Naval Ordnance Test Station.



MADE IN U.S.A.

If the trail offsets obeyed equations (66) and (67) exactly, then the trail calibration constants k_a and k_g could be determined by single measurements using the above formulas. However, the trail offsets do not have this exact hyperbolic dependence on range current. This matter will be taken up in a later section.

MAGNITUDE ERRORS IN THE PREDICTED LEAD

The errors present in an actual sight are due to many different effects. Most of these effects produce errors in both magnitude and direction of the predicted lead. In the present section an attempt will be made to describe the magnitude errors in the gyro-predicted lead. In particular the magnitude errors in the kinematic lead are described in terms of the modified sight sensitivity.

SENSITIVITY OF AN ACTUAL SIGHT

An actual sight shows sensitivity dependence on turning rate of the aircraft as well as on the range current. Figure 12 (taken from reference 12) shows that the variation of sensitivity with angular rate increases as the range current decreases. The decrease in sensitivity at low angular rates for a given range current is explained as being due to friction at the Hooke's joint. The increase in sensitivity for a given range current at high turning rates is explained by the reduction of the electromagnetic constraining torque due to distortion of the eddy current pattern by the secondary magnetic field produced by the eddy currents. The presence of an anomalous up-turning of the constant I_R curves with decreasing turning rate at extremely low values of ω depends on the relative positions of the magnetic and friction centers of the gyro and the direction in which the kinematic lead is generated. The following section will give more detailed discussions of the above-mentioned effects as well as other effects such as air drag, temperature of the dome, presence of trail currents, and optical dip.

Friction at the Hooke's Joint. Certain previous attempts (references 3 and 15) to explain the effect of friction at the Hooke's joint have involved the assumption that the resultant frictional torque is proportional to the deflection of the gyro axis. These analyses, however, were developed in such a manner as to imply that the sensitivity is independent of the turning rate of the aircraft.

PRELIMINARY DATA

19

This material is not to be reproduced and is transmitted for the exclusive use of the indicated recipient. The data presented are tentative and subject to later revision or deletion. The opinions and conclusions expressed herein are those of the individual preparing this report and do not necessarily represent the views of the Naval Ordnance Test Station.

357.11 ALUFEL & GESSER CO.
 10 X 10 to the 1/2 inch, 5th lines accented.
 MADE IN U. S. A.

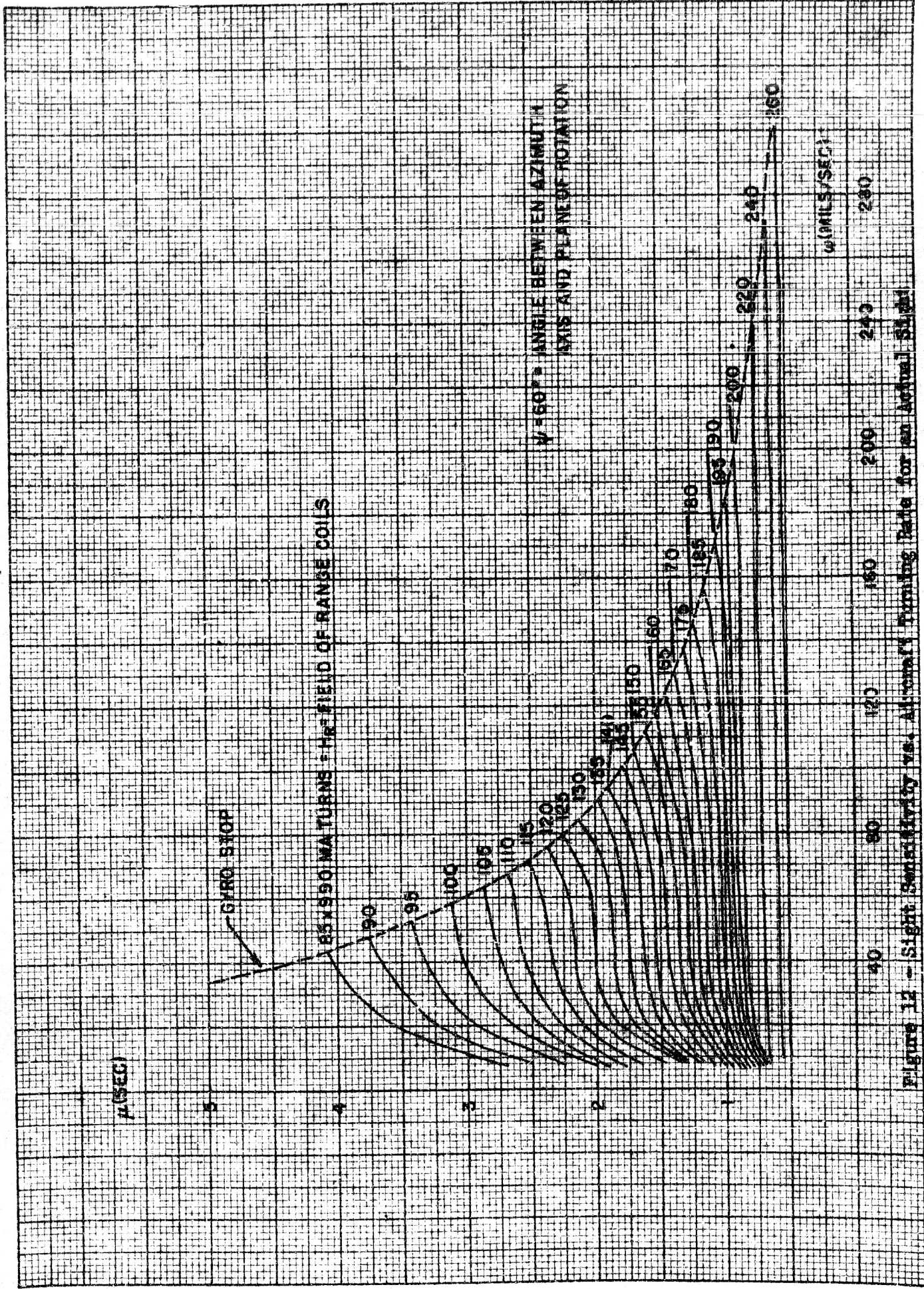


Figure 14 - Sight Sensitivity vs. Azimuth Turning Rate for an Azimuth Sight

The present discussion briefly outlines the assumptions and method for determining the frictional torque given in reference 16 in order to derive an expression for the sensitivity which shows the greater influence of friction at the lower angular rates.

The detailed analysis of the effect of the frictional forces, as they exist in practice in the presence of lubrication, was considered too difficult to pursue and not warranted in view of the ultimate aims of reference 16. However, an upper limit on the frictional forces is obtained by assuming that the rubbing occurs between solid non-lubricated pivot and bearing surfaces. Therefore only normal forces are assumed to exist. The normal force at a pivot and bearing interface is composed of a component of the gravitational force due to the mass of the gyro and a component of the driving force supplied by the drive motor. The coefficients of friction are taken as constant and thus independent of the relative velocities of the rubbing surfaces. Actually the problem is further complicated by the fact that the driving forces are in turn dependent upon the frictional forces. However, this complexity is removed by the approximation that because the gyro spin in the present system is not heavily resisted, the frictional force due to the weight predominates over the frictional force due to the driving force for all but a small part of each revolution. The average effect over a complete revolution of the gyro axis is computed approximately for the case where the deflection of the gyro axis is small.

The result of the analysis of reference 16 gives the approximate frictional torque averaged over a complete revolution as a constant value of

$$T_f \approx 2mgdf \quad (68)$$

where m is the mass of the gyro, g is the acceleration due to gravity, d is an effective radius of the pivot surface, and f is an effective coefficient of friction. The vector T_f lies approximately in the plane of deflection of the gyro axis and is perpendicular to and directed toward the mechanical rest axis. The component $(T_f)_s$ of T_f along the gyro axis opposes the spin vector S and therefore tends to retard the spin. Thus

$$(T_f)_s \approx 2mgdf \sin \theta \quad (69)$$

PRELIMINARY DATA

This material is not to be reproduced and is transmitted for the exclusive use of the indicated recipient. The data presented are tentative and subject to later revision or deletion. The opinions and conclusions expressed herein are those of the individual preparing this report and do not necessarily represent the views of the Naval Ordnance Test Station.

The component $(T_F)_P$ is perpendicular to the gyro axis and is responsible for precessing the gyro toward the mechanical rest axis. Thus

$$(T_F)_P = 2mgdf \cos \theta \quad (70)$$

For small gyro deflections the frictional precession is

$$(T_F)_P = 2mgdf \left(1 - \frac{\theta^2}{2}\right) \quad (71)$$

Now generalizing Newton's second law to include the frictional torque, equation (33) becomes

$$MS \ddot{\eta} = T_E + (T_F)_P \quad (72)$$

Substituting for the eddy current and frictional torques from equations (49) and (71) one obtains

$$MS \ddot{\eta} = \frac{MSI_D^2}{K^2} \theta + 2mgdf \left(1 - \frac{\theta^2}{2}\right) \quad (73)$$

An approximate result is obtained by neglecting the θ^2 term and thus assuming an essentially constant frictional torque. Since $\theta = (1 + a) \lambda_G$ and from equation (52) $\dot{\eta} = \omega - (1 + a) \lambda_G$, the gyro-predicted lead for the steady state (i.e., $\dot{\lambda}_G = 0$) in the presence of friction may be written as

$$\lambda = \frac{K^2}{(1 + a)I_R^2} \left(1 - \frac{2mgdf}{MS} \frac{1}{\omega}\right) \omega \quad (74)$$

where hereafter the subscript G on λ_G is dropped.

PRELIMINARY DATA

This material is not to be reproduced and is transmitted for the exclusive use of the indicated recipient. The data presented are tentative and subject to later revision or deletion. The opinions and conclusions expressed herein are those of the individual preparing this report and do not necessarily represent the views of the Naval Ordnance Test Station.

By introducing the ideal sight sensitivity μ the gyro-predicted lead becomes

$$\lambda = \mu \left(1 - \frac{c_F}{\omega}\right) \omega \quad (75)$$

where

$$c_F = \frac{mgdf}{MS} \quad (76)$$

Therefore the sight sensitivity, as modified by pivot-bearing friction becomes

$$\mu_F = \mu \left(1 - \frac{2c_F}{\omega}\right) \quad (77)$$

A further refinement would involve the retention of the θ^2 term in equation (73).

Malalignment of Friction and Magnetic Centers. The actual sight sensitivity versus angular rate curves of Figure 13 for clockwise and counterclockwise rotation demonstrate the malalignment of friction and magnetic centers. Thus Figure 13(b) contains the friction center of the sight. As the angular rate is reduced the lead and sensitivity decreases until the friction center is reached. Then because the frictional torque is comparable to the eddy current torque for low rates, the gyro axis tends to linger at the friction center and maintain the same deflection as the rate is reduced further. Thus the sensitivity $\mu = \lambda/\omega$ increases again for further decrease of ω . Figure 13(a) obviously does not contain the friction center.

Air Drag on the Dome. Previous analyses (references 3 and 6) have considered only the symmetric air drag on the dome where the torque was assumed to be proportional to the square of the spin velocity. The torque leads to a reduction of the sight sensitivity. However, the writer believes that the asymmetric air drag on the dome due to its proximity to the range coil retaining wall is much more important than the symmetric drag and has the effect of increasing the sight sensitivity for low range coil currents.

PRELIMINARY DATA

This material is not to be reproduced and is transmitted for the exclusive use of the indicated recipient. The data presented are tentative and subject to later revision or deletion. The opinions and conclusions expressed herein are those of the individual preparing this report and do not necessarily represent the views of the Naval Ordnance Test Station.

599-11 KEUFFEL & ESSER CO.
10 X 10 to the 1/2 inch, 5th lines accented.
MADE IN U. S. A.

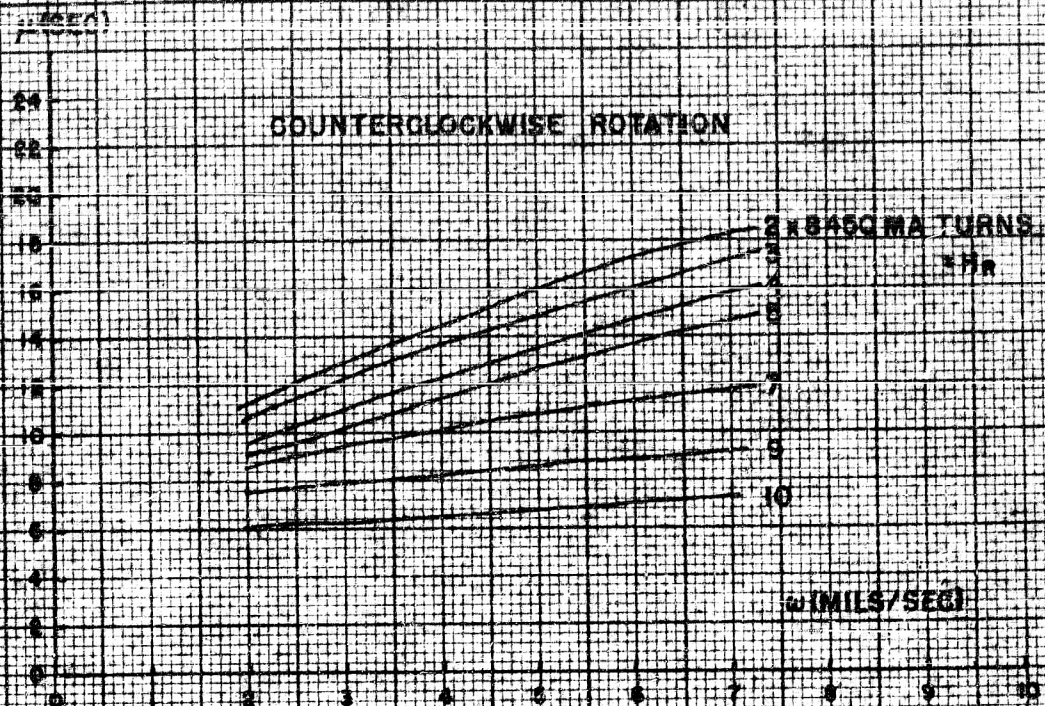


Figure 13(a)
Experimental Sensitivity Curves for Low Angular Rates
and Low Range Currents

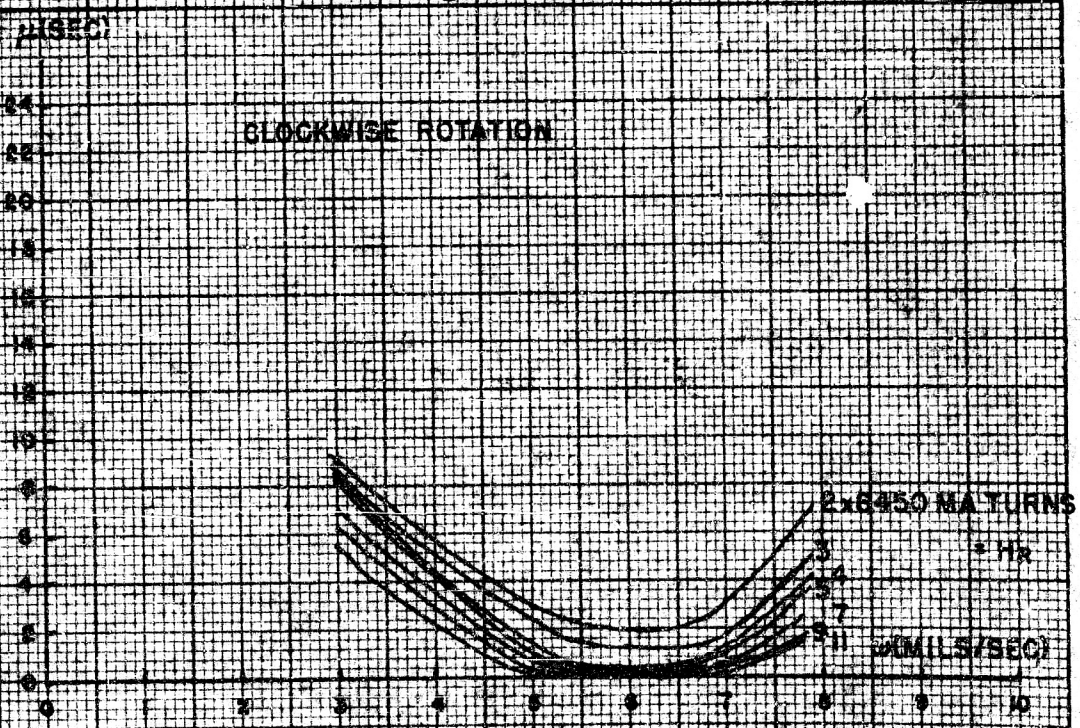


Figure 13(b)
Experimental Sensitivity Curves Showing Displacement
of Friction Center from Magnetic Center

The effect of asymmetric air drag on the dome may be seen by referring to Figure 14. The gyro is shown deflected through the angle θ such that a larger surface area of the dome is under the range coil retaining wall on the right than on the left. The air drag on the spinning dome in the open central region would be negligible compared to that under the range coil retaining wall. This fact is apparent from consideration of the formula for the viscous drag force exerted by a fluid contained between two parallel planes one of which is moving with a velocity v . The force is

$$dF = \frac{\gamma}{y} dA v \quad (78)$$

where γ is the coefficient of viscosity, dA is an element of area, and y is the spacing between the wall and the dome. This expression neglects slip and assumes that the air adjacent to the dome has the velocity of the dome and that the air adjacent to the retaining wall is at rest.

Since the area of dome under the retaining wall is proportional to the integrated line element $Rd\phi$

$$dA = \gamma R d\phi \quad (79)$$

From Figure 14

$$v = SR \sin \phi \quad (80)$$

and therefore

$$dF = \frac{\gamma SR^2}{y} \sin \phi d\phi \quad (81)$$

To further simplify the analysis $\sin \phi$ is replaced by ϕ so that the aerodynamic drag force on the right side of the dome becomes

$$\begin{aligned} F_1 &= \frac{\gamma SR^2}{y} \int_{\theta_c}^{\theta_D} \phi d\phi = \frac{\gamma SR^2}{2y} (\theta_D^2 - \theta_c^2) \\ &= \frac{\gamma SR^2}{2y} [\theta_D^2 - (\theta_c - \theta)^2] \quad (82) \end{aligned}$$

PRELIMINARY DATA

23

This material is not to be reproduced and is transmitted for the exclusive use of the indicated recipient. The data presented are tentative and subject to later revision or deletion. The opinions and conclusions expressed herein are those of the individual preparing this report and do not necessarily represent the views of the Naval Ordnance Test Station.

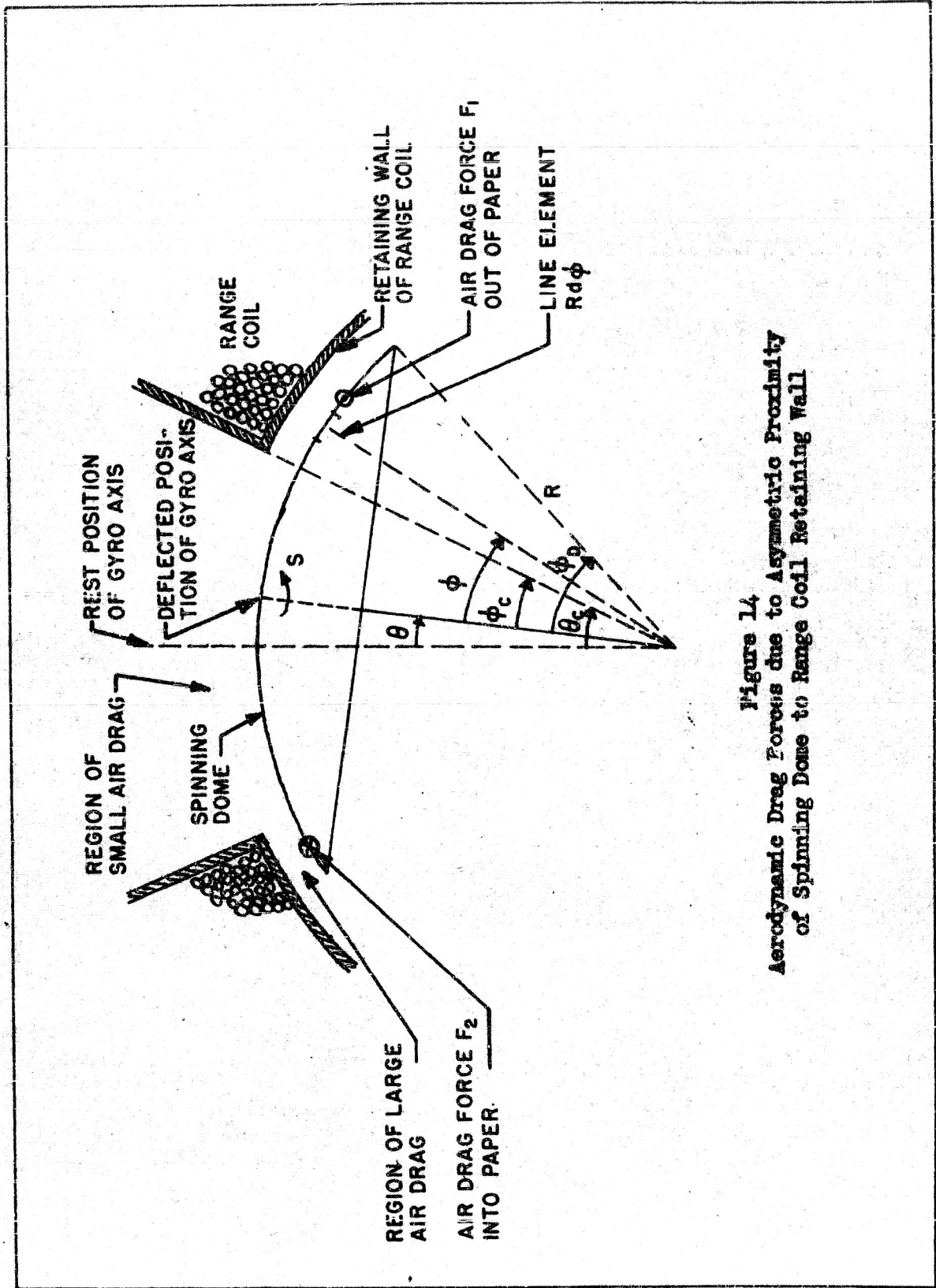


Figure 14
 Aerodynamic Drag Forces due to Asymmetric Proximity
 of Spinning Dome to Range Coil Retaining Wall

Similarly the force on the left side of the dome is

$$F_2 = \frac{\sigma I G R^2}{2y} \left[\theta_D^2 - (\theta_c + \theta)^2 \right] \quad (83)$$

The forces F_1 and F_2 produce an unbalanced couple which may be replaced by a single resultant force

$$F_R = F_1 - F_2 = \frac{2\sigma I R^2 \theta_c}{y} \theta \quad (84)$$

acting at some point perpendicular to the line passing through F_1 and F_2 . The direction of F_R is in the direction of F_1 . This results in an aerodynamic torque

$$\underline{T}_A = \underline{R} \times \underline{F}_R \quad (85)$$

which opposes the eddy current restoring torque. By letting the constant

$$A = \frac{2\sigma I R^3 \theta_c}{y} \quad (86)$$

the torque becomes

$$T_A = A\theta \quad (87)$$

Application of Newton's second law of motion again gives

$$MS\ddot{\eta} = T_E + T_F - T_A \quad (88)$$

which results in a steady state lead

$$\lambda = \mu \frac{(1 - \frac{C_F}{\sigma})}{(1 - \frac{A}{MS} \frac{K^2}{I_R})} \omega \quad (89)$$

PRELIMINARY DATA

This material is not to be reproduced and is transmitted for the exclusive use of the indicated recipient. The data presented are tentative and subject to later revision or deletion. The opinions and conclusions expressed herein are those of the individual preparing this report and do not necessarily represent the views of the Naval Ordnance Test Station.

or a sensitivity of

$$\mu_A = \mu \frac{(1 - \frac{c_F}{\omega})}{(1 - \frac{c_A}{I_R^2})} \quad (90)$$

where

$$c_A = \frac{AK^2}{ES} \quad (91)$$

Thus from equation (90) it is clear that the sensitivity is increased by asymmetric air drag for low range coil currents. No quantitative measurements of c_A have been made, but in the event that the term $c_A/I_R^2 \ll 1$ the sensitivity becomes

$$\mu_A = \mu (1 - \frac{c_F}{\omega}) (1 + \frac{c_A}{I_R^2}) \quad (92)$$

Reduction of Electromagnetic Constraint Due to Large Eddy Currents.

This section discusses the case in which the eddy currents induced in the dome are sufficiently large to create a secondary magnetic induction B_S which is not negligible compared to the primary induction B . The secondary field distorts the eddy current pattern induced by the primary field in such a manner as to reduce the restoring torque. The torque is also misdirected, which effect will be described in the section on magnetic dip. The expression for the reduced electromagnetic constraining torque is developed according to the following general outline:

The resultant induction B_r is the superposition of the primary and secondary inductions. Thus

$$\underline{B}_r = \underline{B} + \underline{B}_S \quad (93)$$

Due to the motion of the conducting dome through the resultant induction B_r an electric field E is established in the dome. A modification of Faraday's empirical law of induction gives the

PRELIMINARY DATA

This material is not to be reproduced and is transmitted for the exclusive use of the indicated recipient. The data presented are tentative and subject to later revision or deletion. The opinions and conclusions expressed herein are those of the individual preparing this report and do not necessarily represent the views of the Naval Ordnance Test Station.

connection between \underline{B}_T and \underline{E} as

$$\nabla \times \underline{E} = - \frac{\partial \underline{B}_T}{\partial t} \quad (94)$$

The eddy current density \underline{i} which results from the electric field is given by Ohm's law as

$$\underline{i} = \sigma \underline{E} \quad (95)$$

where σ is the conductivity of the dome. Substituting for the electric field in the law of induction gives

$$\nabla \times \underline{i} = - \sigma \frac{\partial \underline{B}_T}{\partial t} \quad (96)$$

The eddy current density is connected to the secondary induction by the relation

$$4\pi \mu \underline{i} = \nabla \times \underline{B}_S \quad (97)$$

wherein $\underline{B}_S = \mu \underline{H}_S$ in a region of permeability μ . Taking the curl of both sides of equation (97) and expanding according to the rules of vector analysis gives

$$4\pi \mu \nabla \times \underline{i} = \nabla \times (\nabla \times \underline{B}_S) = - \nabla^2 \underline{B}_S + \nabla (\nabla \cdot \underline{B}_S) \quad (98)$$

Since \underline{B}_S is solenoidal the divergence vanishes, i.e.

$$\nabla \cdot \underline{B}_S = 0 \quad (99)$$

and substitution of equation (98) into equation (96) with the separation of the total induction \underline{B}_T into its components \underline{B} and \underline{B}_S by equation (93) yields

$$\frac{1}{4\pi \sigma \mu} \nabla^2 \underline{B}_S = \frac{\partial \underline{B}}{\partial t} + \frac{\partial \underline{B}_S}{\partial t} \quad (100)$$

PRELIMINARY DATA

This material is not to be reproduced and is transmitted for the exclusive use of the indicated recipient. The data presented are tentative and subject to later revision or deletion. The opinions and conclusions expressed herein are those of the individual preparing this report and do not necessarily represent the views of the Naval Ordnance Test Station.

If the spacial distribution of the primary induction B is obtained, then the form of the secondary induction may be inferred from the second order "wave" equation (100). Knowing the form of B_p one may obtain the eddy current density from equation (97).

The product of the eddy current density i and the primary induction B is integrated over the volume traversed by the eddy currents to obtain the force, which when properly combined with the forces from the other three pairs of poles gives the resultant force on the dome. An alternative method of calculating the force is to first calculate the electrical power i^2R dissipated by the eddy currents in the dome. Then the power is divided by the velocity of the region of the dome under a pole gap to obtain the force. After multiplication of the total resultant force by the lever arm, which in this case is the radius of the dome, one finally obtains the desired electromagnetic constraining torque.

A rigorous calculation of the primary induction B at an arbitrary point on the surface of the spinning dome was attempted without success due to difficulty in handling the resulting integrals. Nevertheless the set up for the calculation is presented with the hope that someone's future efforts will be more successful.

Referring to Figure 15 the problem is to calculate the primary induction B at the arbitrary point Q for an arbitrary deflection of the gyro axis from the geometrical center of the gyro housing as indicated by the angles θ_g and ψ . The plane circular end of the magnetic pole of radius a is a distance h above the dome and at an angle θ_p with respect to the housing center. Following the method of Smythe who developed an approximate solution for the analogous problem (see reference 23) of a spinning disc, one may set up the scalar magnetic potential at Q as

$$\Omega = \frac{\Phi}{(2\pi a)^2} \int \frac{dS}{R} \quad (101)$$

where Φ is the total flux emerging normally from the pole face. The differential dS is an element of area of the pole face, and R is the distance from dS to the arbitrary point Q on the surface of the dome. The gradient of Ω will yield the desired field.

From the figure R is obtained as

PRELIMINARY DATA

This material is not to be reproduced and is transmitted for the exclusive use of the indicated recipient. The data presented are tentative and subject to later revision or deletion. The opinions and conclusions expressed herein are those of the individual preparing this report and do not necessarily represent the views of the Naval Ordnance Test Station.

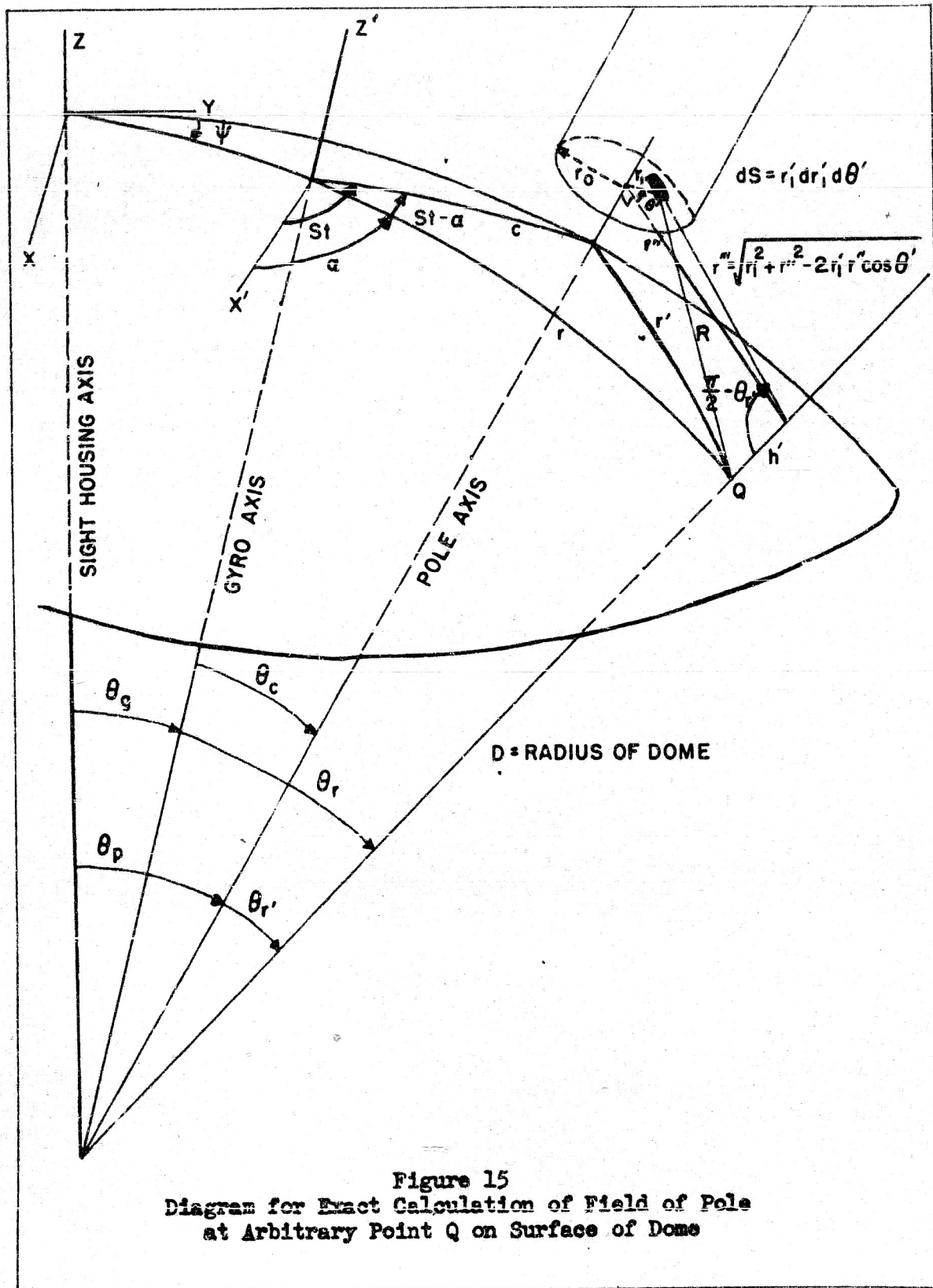


Figure 15
 Diagram for Exact Calculation of Field of Pole
 at Arbitrary Point Q on Surface of Dome

$$R = \sqrt{h'^2 + r''^2 - 2h' r'' \sin \theta'_r} \quad (102)$$

where

$$r'' = \sqrt{r_1'^2 + r''^2 - 2r_1' r'' \cos \theta'} \quad (103)$$

$$r'' = (h + D) \tan \theta'_r \quad (104)$$

$$\cos \theta'_r = \cos \theta_r \cos \theta_c + \sin \theta_r \sin \theta_c \cos(\omega t - \alpha) \quad (105)$$

$$\cos \theta_c = \cos \theta_p \cos \theta_g + \sin \theta_p \sin \theta_g \cos \psi \quad (106)$$

Thus R may be expressed in terms of the constants θ_p , h , and D and the primary variables θ_g , ψ , and t . For the results of a somewhat similar but simpler integration the reader is referred to the above-mentioned reference to Smythe's work.

The remainder of this section will be concerned with a somewhat less accurate but considerably more enlightening solution of the problem essentially as suggested by Rudenberg (reference 24) and applied to the eddy current constrained gyroscope by Brink (reference 25).

For simplicity the geometry of Figure 15 is replaced by that of Figure 16, wherein a thin conducting sheet bounded by straight lines moves lengthwise in the narrow gap between a pair of magnetic poles with square faces. The spacial distribution of the primary magnetic induction B is assumed to be cosinusoidal and therefore of limited extent, namely a square area of side b , on the conducting sheet. Let

$$B = B_0 \cos \frac{\pi}{b} x \cos \frac{\pi}{b} y \quad (107)$$

Only the z component of induction is considered since the other components should have negligible effects if the sheet is sufficiently thin. Since the sheet is moving in the positive x direction with a velocity v , then at a time t after a certain point on the sheet passes through $x = 0$, the induction at that point will be

$$B = B_0 \cos \frac{\pi}{b} (x + vt) \cos \frac{\pi}{b} y \quad (108)$$

PRELIMINARY DATA

This material is not to be reproduced and is transmitted for the exclusive use of the indicated recipient. The data presented are tentative and subject to later revision or deletion. The opinions and conclusions expressed herein are those of the individual preparing this report and do not necessarily represent the views of the Naval Ordnance Test Station.

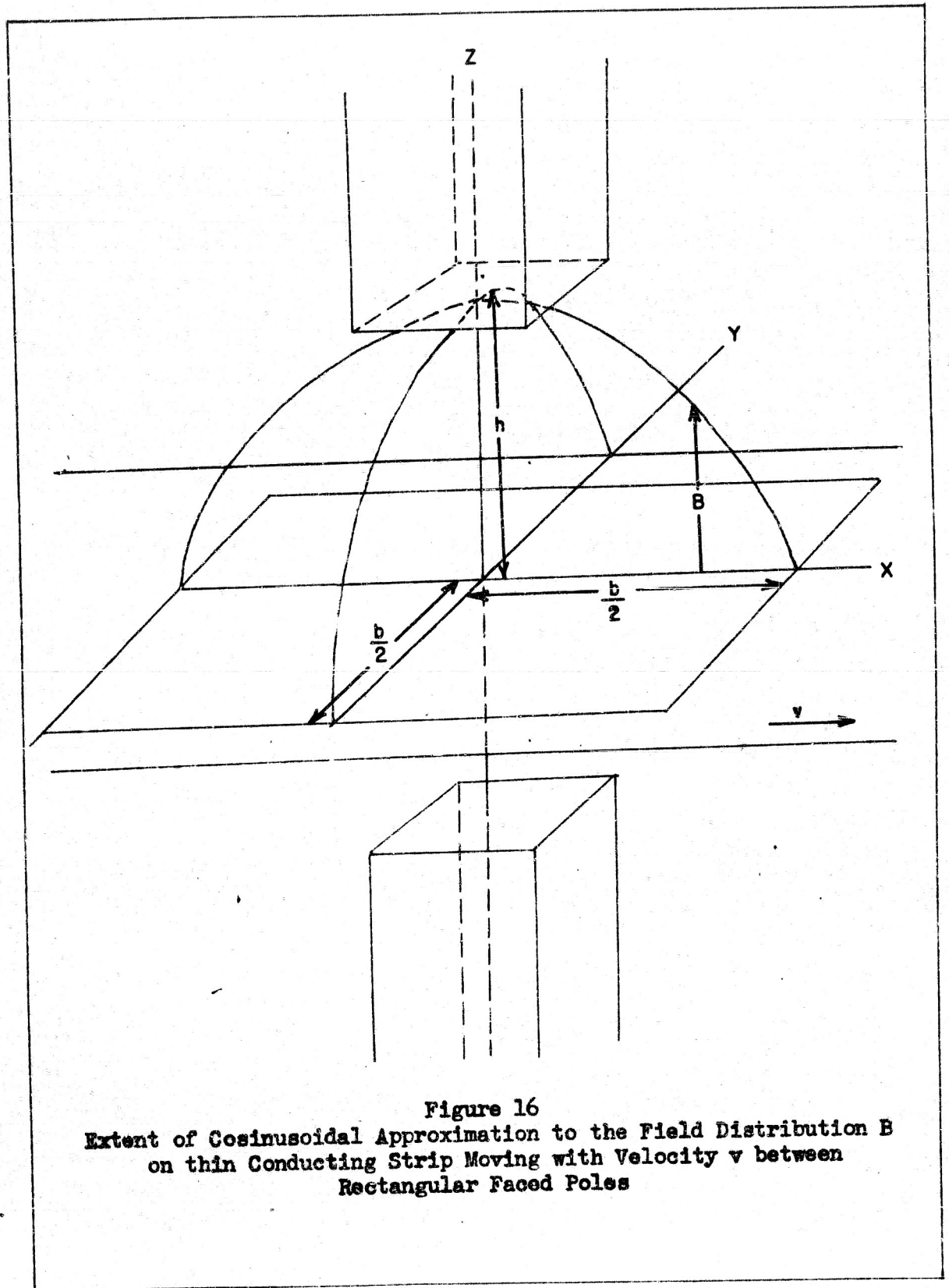


Figure 16
Extent of Cosinusoidal Approximation to the Field Distribution B
on thin Conducting Strip Moving with Velocity v between
Rectangular Faced Poles

Rather than follow the physically causal sequence that the primary field produces the eddy currents which in turn produce the secondary field, it is easier to determine the secondary field first from equation (100) and then determine the eddy currents from equation (97). Thus the time derivative of B needed for the "wave" equation (100) is

$$\frac{\partial B}{\partial t} = -\frac{\pi}{b} v B_0 \sin \frac{\pi}{b}(x + vt) \cos \frac{\pi}{b} y \quad (109)$$

Consequently equation (100) reads

$$\frac{1}{4\pi\sigma\mu} \nabla^2 B_s - \frac{\partial B_s}{\partial t} = -\frac{\pi}{b} v B_0 \sin \frac{\pi}{b}(x + vt) \cos \frac{\pi}{b} y \quad (110)$$

It is reasonable to expect the secondary induction B_s on the sheet to be in the z direction and have the same spacial distribution $[\cos(\pi y/b)]$ perpendicular to the motion as the primary induction B. However, the distribution of B_s in the x direction of motion will be shifted and therefore should contain sine as well as cosine terms. These considerations suggest the form of the secondary induction as

$$B_s = C_1 \sin \frac{\pi}{b}(x + vt) \cos \frac{\pi}{b} y + C_2 \cos \frac{\pi}{b}(x + vt) \cos \frac{\pi}{b} y \quad (111)$$

with the constants C_1 and C_2 to be determined. Substitution of equation (111) into equation (110) is now performed using the Laplacian in rectangular coordinates as

$$\nabla^2 B_s = \frac{\partial^2 B_s}{\partial x^2} + \frac{\partial^2 B_s}{\partial y^2}$$

The result is

$$\begin{aligned} & \left(\frac{\pi}{2\sigma\mu b^2} C_1 - \frac{\pi v}{b} C_2 - \frac{\pi}{b} v B_0 \right) \sin \frac{\pi}{b}(x + vt) \cos \frac{\pi}{b} y \\ & + \left(\frac{\pi}{2\sigma\mu b^2} C_2 + \frac{\pi v}{b} C_1 \right) \cos \frac{\pi}{b}(x + vt) \cos \frac{\pi}{b} y = 0 \end{aligned} \quad (112)$$

PRELIMINARY DATA

29

This material is not to be reproduced and is transmitted for the exclusive use of the indicated recipient. The data presented are tentative and subject to later revision or deletion. The opinions and conclusions expressed herein are those of the individual preparing this report and do not necessarily represent the views of the Naval Ordnance Test Station.

Since the coefficients of the trigonometric terms are independent, they must vanish identically thus giving two relations to be solved simultaneously for C_1 and C_2 . The results are

$$\left. \begin{aligned} C_1 &= \frac{2\sigma\mu b v B_0}{1 + 4\sigma^2\mu^2 b^2 v^2} = \frac{\delta v B_0}{1 + (\delta v)^2} \\ C_2 &= \frac{-4\sigma^2\mu^2 b^2 v^2 B_0}{1 + 4\sigma^2\mu^2 b^2 v^2} = \frac{-(\delta v)^2 B_0}{1 + (\delta v)^2} \end{aligned} \right\} \quad (113)$$

where

$$\delta = 2\sigma\mu b \quad (114)$$

The eddy currents may now be calculated from equation (97) which when expanded gives

$$\begin{aligned} \underline{i} &= \frac{1}{4\pi\mu} \hat{i} \left(\frac{\partial B_{zz}}{\partial y} - \frac{\partial B_{zy}}{\partial z} \right) + \frac{1}{4\pi\mu} \hat{j} \left(\frac{\partial B_{zx}}{\partial z} - \frac{\partial B_{xz}}{\partial x} \right) \\ &+ \frac{1}{4\pi\mu} \hat{k} \left(\frac{\partial B_{zy}}{\partial x} - \frac{\partial B_{zx}}{\partial y} \right) \end{aligned} \quad (115)$$

where \hat{i} , \hat{j} , and \hat{k} are unit vectors along the x, y, z axes, respectively.

Since B_0 is only of consequence in the z direction at the surface of the sheet, certain terms in equation (115) vanish. Therefore

$$\left. \begin{aligned} i_x &= \frac{1}{4\pi\mu} \frac{\partial B_z}{\partial y} = -\frac{1}{4\pi\mu b} \left[C_1 \sin \frac{\pi}{b}(x + vt) + C_2 \cos \frac{\pi}{b}(x + vt) \right] \sin \frac{\pi}{b} y \\ i_y &= -\frac{1}{4\pi\mu} \frac{\partial B_z}{\partial x} = -\frac{1}{4\pi\mu b} \left[C_1 \cos \frac{\pi}{b}(x + vt) - C_2 \sin \frac{\pi}{b}(x + vt) \right] \cos \frac{\pi}{b} y \\ i_z &= 0 \end{aligned} \right\} \quad (116)$$

PRELIMINARY DATA

This material is not to be reproduced and is transmitted for the exclusive use of the indicated recipient. The data presented are tentative and subject to later revision or deletion. The opinions and conclusions expressed herein are those of the individual preparing this report and do not necessarily represent the views of the Naval Ordnance Test Station.

From equations (113)

$$C_2 = -\delta v C_1 \quad (117)$$

Thus

$$i_x = -\frac{C_1}{4\mu b} \left[\sin \frac{\pi}{b}(x + vt) - \delta v \cos \frac{\pi}{b}(x + vt) \right] \sin \frac{\pi}{b} y$$

$$i_y = -\frac{C_1}{4\mu b} \left[\cos \frac{\pi}{b}(x + vt) + \delta v \sin \frac{\pi}{b}(x + vt) \right] \cos \frac{\pi}{b} y \quad (118)$$

$$i_z = 0$$

Introducing the phase angle

$$\phi = \tan^{-1} \delta v \quad (119)$$

and the amplitude

$$i_0 = \frac{C_1}{4\mu b} \sqrt{1 + (\delta v)^2} = \frac{\delta v B_0}{4\mu b \sqrt{1 + (\delta v)^2}} \quad (120)$$

equations (118) become

$$i_x = -i_0 \sin \left[\frac{\pi}{b}(x + vt) - \phi \right] \sin \frac{\pi}{b} y$$

$$i_y = -i_0 \cos \left[\frac{\pi}{b}(x + vt) - \phi \right] \cos \frac{\pi}{b} y \quad (121)$$

$$i_z = 0$$

More is said about the significance of this phase angle ϕ in the section on magnetic dip.

PRELIMINARY DATA

This material is not to be reproduced and is transmitted for the exclusive use of the indicated recipient. The data presented are tentative and subject to later revision or deletion. The opinions and conclusions expressed herein are those of the individual preparing this report and do not necessarily represent the views of the Naval Ordnance Test Station.

Since the eddy currents of equation (121) produce a drag force on the conducting sheet and therefore tend to slow it down, an equal and opposite force must be applied to the sheet to maintain its motion with a velocity v . Also, the power P , or mechanical work done per unit time, is equal to the rate of heating $i^2 R$ of the sheet. Here the effects of other drag forces such as mechanical and aerodynamic friction are neglected. Thus the drag force of the eddy currents is

$$F = \frac{P}{v} = \frac{i^2 R}{v} = \frac{1}{v} \int_{-b/2}^{+b/2} \int_{-b/2}^{+b/2} \int_{-\tau/2}^{+\tau/2} \frac{i^2}{\sigma} dx dy dz \quad (122)$$

where τ is the thickness of the conducting sheet. Since the total eddy current i may be obtained from

$$i^2 = i_x^2 + i_y^2 + i_z^2 \quad (123)$$

substitution of equations (123), (121), (120), and (114) into equation (122) and integration gives the drag force as

$$F = \frac{1/8 \tau \sigma v b^2 B_0^2}{1 + 4\sigma^2 \mu^2 b^2 v^2} \quad (124)$$

The role of the pole gap spacing $l = 2h$ in Figure 16 is introduced into equation (124) by replacing the permeability μ in the denominator by the ratio of sheet thickness τ to pole gap spacing l . A qualitative argument for this is given on Page 288 of reference 24. Therefore

$$\mu \approx \frac{\tau}{l} \quad (125)$$

Then the force becomes

$$F = \frac{1/8 \tau \sigma v b^2 B_0^2}{1 + 4\sigma^2 \frac{\tau^2}{l^2} b^2 v^2} \quad (126)$$

PRELIMINARY DATA

This material is not to be reproduced and is transmitted for the exclusive use of the indicated recipient. The data presented are tentative and subject to later revision or deletion. The opinions and conclusions expressed herein are those of the individual preparing this report and do not necessarily represent the views of the Naval Ordnance Test Station.

Following Brink (see reference 25) the above equation for the drag force on a conducting sheet translating linearly in a pole gap with poles of rectangular cross section is now applied to the geometry of Figure 15 for a spinning dome in the air gap field of magnetic poles with circular pole faces. The reasonable assumption is made that the expression for the drag force will have the same general form as equation (126).

The side b of the square boundary of the field distribution on the rectangular sheet is assumed proportional to the radius r_0 of an equivalent circular area which would contain all the cosinusoidally distributed flux from an equivalent circular pole. Thus $b \sim r_0$. Or further it may be assumed that this circular area may be replaced by another one of radius r_p containing all the flux from an equivalent pole of radius r_p , where the flux is constant over the whole area $A = \pi r_p^2$ but produces the same effect as the original flux distribution. Thus $b \sim \sqrt{A}$, also v is replaced by the product of the gyro spin velocity S and its lever arm $D \sin \theta$ and B_0 by μH .

Finally the restoring torque is obtained as

$$\underline{T} = \underline{D} \times \underline{F} = \frac{k_1 \tau \sigma A D^2 \mu^2 H^2 S \sin \theta}{1 + k_2 A \left(\frac{\sigma \tau D}{L} \right)^2 S^2 \sin^2 \theta} = \frac{g_1 S H^2 \theta}{1 + g_2 \theta^2} \quad (127)$$

It is apparent that the last term in the denominator provides the distortion to the more elementary expression derived in an earlier section. The restoring torque T is reduced most at large gyro deflections for a given geometry described by L , τ , D , and A and a given spin velocity S .

Using equation (127) to calculate the sensitivity one obtains

$$\mu_b = \frac{I(1 + g_2 \theta^2)}{(1 + a)g_1 H^2}$$

This distortion of the eddy current pattern for large deflections is believed to be the chief cause for the turning up of the sensitivity curves for low I_p and high ω as shown in Figure 12.

PRELIMINARY DATA

This material is not to be reproduced and is transmitted for the exclusive use of the indicated recipient. The data presented are tentative and subject to later revision or deletion. The opinions and conclusions expressed herein are those of the individual preparing this report and do not necessarily represent the views of the Naval Ordnance Test Station.

Another possible contributing factor to the turning up of the above-mentioned curves is that a considerable portion of the flux "spills over" the edge of the dome for large gyro deflections thus reducing the restoring torque disproportionately to the decrease in the square of the range coil current. Evidence that the magnetic field is not confined to the pole gaps has been obtained in measurements of the static field distribution for a non-spinning dome. See reference 26.

Temperature Variation in the Dome. Temperature variations in the metal dome cause changes in conductivity and thus restrict or augment the eddy current flow thus altering the restoring torque and finally the gyro deflection. Since by equation (59) the sensitivity is given by

$$\mu = \frac{K^2}{(1 + a)I_R^2}$$

and the dependence of K on conductivity is given by equation (47) as

$$\frac{K^2}{I_R^2} = \frac{C_T^2}{\rho}$$

where C_T is a constant, then

$$K = C_T \sqrt{\rho} \tag{128}$$

where ρ is the resistivity of the dome material. The resistivity ρ at any temperature t is expressed as a function of the resistivity ρ_r at some reference temperature t_r by the relation

$$\rho = \rho_r [1 + \alpha_r (t - t_r)] \tag{129}$$

where α_r is the coefficient of resistivity at the temperature t_r . For aluminum $\alpha_r = 0.0034$ at $t_r = 20$ deg C, and therefore since most sights are calibrated when warmed up to approximately 20 deg C above ambient room temperature or 40 deg C and

PRELIMINARY DATA

This material is not to be reproduced and is transmitted for the exclusive use of the indicated recipient. The data presented are tentative and subject to later revision or deletion. The opinions and conclusions expressed herein are those of the individual preparing this report and do not necessarily represent the views of the Naval Ordnance Test Station.

$$\alpha_{40} = \frac{\alpha_{20}}{1 + 20\alpha_{20}} = 0.0032$$

therefore

$$K_{40} = C_T \sqrt{\rho_{40} [1 + 0.0032(t - 40)]} \quad (130)$$

Since the term containing α_{20} is much smaller than unity, the radical is removed by the approximation

$$K \approx K_{40} [1 + 0.0016(t - 40)] \quad (131)$$

where $K_{40} = C_T \sqrt{\rho_{40}}$. Thus the temperature dependent sensitivity becomes

$$\mu = \frac{K_{40}^2}{(1 + a)I_R^2} [1 + 0.0016(t - 40)]^2$$

or approximately

$$\mu = \frac{K_{40}^2}{(1 + a)I_R^2} [1 + 0.0032(t - 40)] \quad (132)$$

The differential change in sensitivity for a small change Δt in temperature is

$$\Delta\mu = \frac{2K_{40}^2}{(1 + a)I_R^2} [1 + 0.0016(t - 40)] \quad (133)$$

Dividing equation (133) by equation (132) to obtain the percentage change in sensitivity per degree centigrade change in dome temperature one obtains

$$\frac{\Delta\mu}{\mu} \times \frac{100}{\Delta t} = \frac{0.0032 \times 100}{1 + 0.00175(t - 15)} \approx 0.32\% \quad (134)$$

PRELIMINARY DATA

This material is not to be reproduced and is transmitted for the exclusive use of the indicated recipient. The data presented are tentative and subject to later revision or deletion. The opinions and conclusions expressed herein are those of the individual preparing this report and do not necessarily represent the views of the Naval Ordnance Test Station.

Presence of Trail Offsets. The presence of trail offset fields has the effect of reducing the sight sensitivity below the ideal value given in equation (59). The form of this reduced sensitivity μ_T may be seen qualitatively by referring to equation (43) for the \overline{GTC} predicted lead. The coefficient of a gives the reduced value of the sensitivity μ_T as

$$\mu_T = \frac{KS}{4Dc(1+a)H_R^2 \left(1 + \frac{H_a^2}{2H_R^2}\right)} \quad (135)$$

In terms of the ideal sensitivity μ , as defined by equation (59) the reduced sensitivity is

$$\mu_T = \frac{K^2}{(1+a)I_R^2} \frac{1}{\left(1 + \frac{H_a^2}{2K_R^2}\right)} = \frac{2\mu}{2 + \epsilon_a^2} \quad (136)$$

where ϵ_a is the ratio of the azimuth trail field to the range coil field. Thus there results a fractional reduction in sensitivity of

$$\frac{\mu - \mu_T}{\mu} = \frac{\epsilon_a^2}{2 + \epsilon_a^2} \quad (137)$$

The more rigorous analysis which follows shows that the actual reduction of sensitivity is slightly larger than that given in equation (137).

The more general case of an arbitrary plane of rotation inclined at an angle ψ to the azimuth axis and the presence of both azimuth and elevation offsets is now considered. The angular relationships of the lead vectors are shown in Figure 17.

From reference 6 the more general equations* for the total lead λ in terms of its components λ_A and λ_G are

* Still more general equations, which take account of the effect of roll (i.e., angular rates perpendicular to the plane determined by the ω_g and ω_A vectors) are given in reference 3.

PRELIMINARY DATA

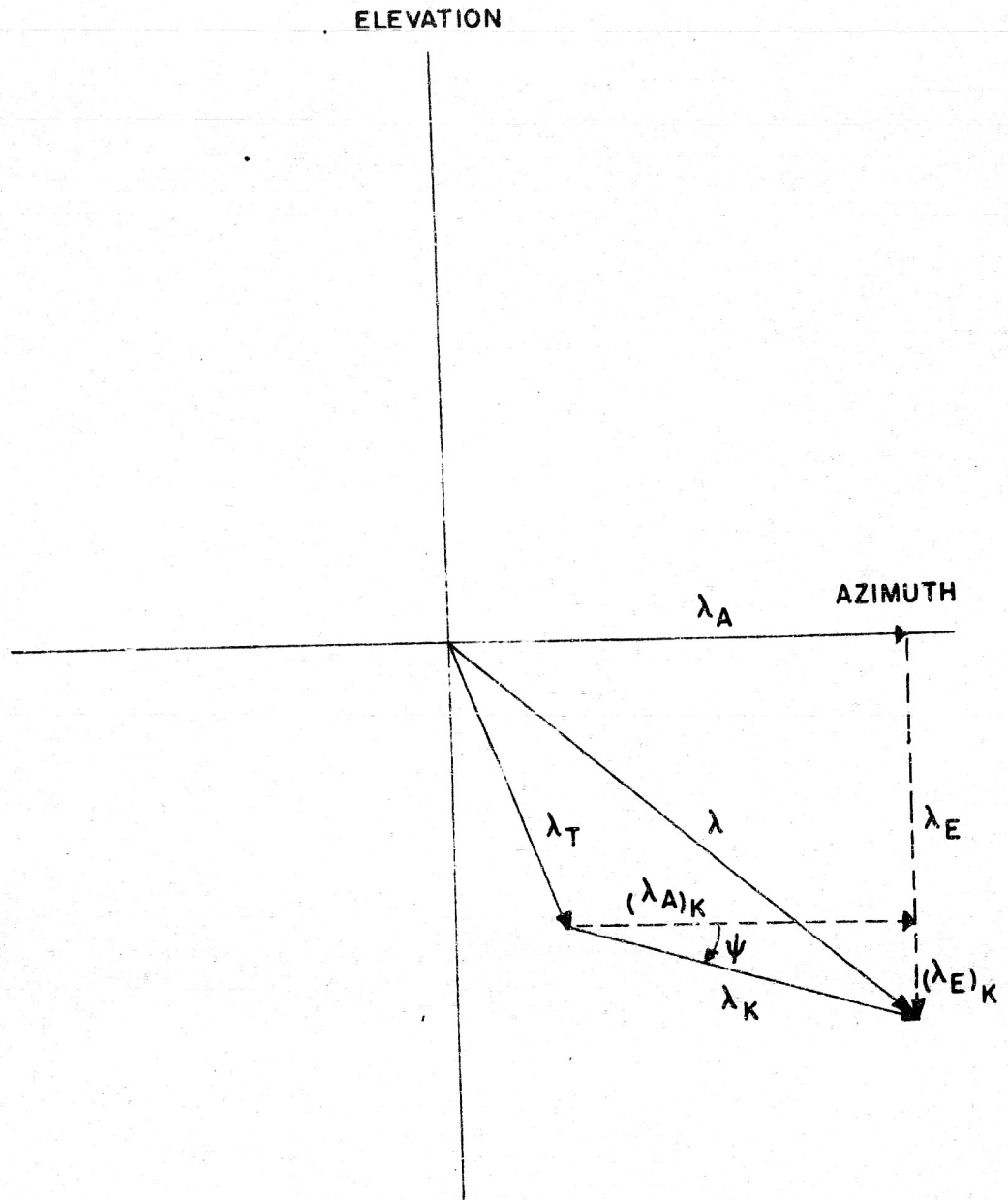


Figure 17
 Angular relations of the lead vectors for
 arbitrary directions of kinematic λ_K and trail offset λ_T

$$(B - D)(1 + a_E) \lambda_E - C(1 + a_A) \lambda_A = K_1 - C_R \omega_E$$

$$C(1 + a_E) \lambda_E + (B + D)(1 + a_A) \lambda_A = K_2 + C_R \omega_A \quad (138)$$

where the signs in front of the "a" values are positive, since in this report "a" is taken as a positive constant. The other symbols are defined as follows:

$$B = 1/2(F_{GX}^P + F_{GY}^P + F_{RZ}^A) + 2k(2H_R^2 + H_a^2 + H_e^2) \cos^2 \theta_p \quad (139)$$

$$C = 1/2(A_G + B_G - C_G)S + \frac{\alpha_1}{S} \quad (140)$$

$$D = k(H_e^2 - H_a^2) \sin^2 \theta_p \quad (141)$$

$$K_1 = 2kHH_e \sin 2\theta_p \quad (142)$$

$$K_2 = 2kHH_a \sin 2\theta_p \quad (143)$$

where

C_R = moment of inertia of gyro rotor about its axis

ω_E, ω_A = elevation and azimuth components of angular speeds of rotation of sight

F_{GX}^P, F_{GY}^P = pivot friction coefficients

F_{RZ}^A = aerodynamic drag coefficient

k = proportionality constant in eddy current torque formula

θ_p = angle between axis of magnetic pole and the axis of symmetry of the magnetic field assembly

A_G, B_G, C_G = moments of inertia of Hooke's joint spider about its x, y, z, axes, respectively.

α_1 = leading coefficient of Venturi torque

37

PRELIMINARY DATA

This material is not to be reproduced and is transmitted for the exclusive use of the indicated recipient. The data presented are tentative and subject to later revision or deletion. The opinions and conclusions expressed herein are those of the individual preparing this report and do not necessarily represent the views of the Naval Ordnance Test Station.

For the present analysis the approximation $a_E \approx a_A \approx a$ is made. Equations (138) may be solved simultaneously for λ_E and λ_A yielding

$$\lambda_E = \frac{-C_R(B+D)}{(1+a)(B^2-D^2+C^2)} \omega_E + \frac{CC_R}{(1+a)(B^2-D^2+C^2)} \omega_A$$

$$+ \frac{K_1(B+D)}{(1+a)(B^2-D^2+C^2)} + \frac{K_2 C}{(1+a)(B^2-D^2+C^2)}$$

and

$$\lambda_A = \frac{-CC_R}{(1+a)(B^2-D^2+C^2)} \omega_E - \frac{C_R(B-D)}{(1+a)(B^2-D^2+C^2)} \omega_A$$

$$+ \frac{K_1 C}{(1+a)(B^2-D^2+C^2)} - \frac{K_2(B-D)}{(1+a)(B^2-D^2+C^2)}$$

(144)

Referring to Figure 17 it is apparent that the elevation and azimuth components of the kinematic lead are of the form

$$\left. \begin{aligned} (\lambda_E)_K &= a_1 \omega_E + a_2 \omega_A \\ (\lambda_A)_K &= b_1 \omega_E + b_2 \omega_A \end{aligned} \right\} \quad (145)$$

In terms of the total angular rate ω equation (145) becomes

$$\left. \begin{aligned} (\lambda_E)_K &= a_1 \omega \sin \psi + a_2 \omega \cos \psi \\ (\lambda_A)_K &= b_1 \omega \sin \psi + b_2 \omega \cos \psi \end{aligned} \right\} \quad (146)$$

The total kinematic lead becomes

PRELIMINARY DATA

This material is not to be reproduced and is transmitted for the exclusive use of the indicated recipient. The data presented are tentative and subject to later revision or deletion. The opinions and conclusions expressed herein are those of the individual preparing this report and do not necessarily represent the views of the Naval Ordnance Test Station.

$$\left. \begin{aligned} \lambda_K &= \sqrt{(\lambda_E)_K^2 + (\lambda_A)_K^2} \\ &= \omega \sqrt{(a_1 \sin \psi + a_2 \cos \psi)^2 + (b_1 \sin \psi + b_2 \cos \psi)^2} \end{aligned} \right\} \quad (147)$$

Since the coefficient of ω is the reduced sight sensitivity, one may show that

$$\mu_T = \frac{C_R}{(1+a)(1 - \frac{D^2 - C^2}{B^2})} \sqrt{1 - \frac{2D}{B} \cos 2\psi + \frac{C^2 + D^2}{B^2} - \frac{2CD}{B^2} \sin 2\psi} \quad (148)$$

The third and fourth terms under the radical are neglected, since they are second order quantities and small compared to the first two terms. The constant C depends on the moments of inertia of the Hooke's joint spider according to equation (140). In this analysis of the dependence of sensitivity on trail currents the effect of C is neglected ($C = 0$). Also the radical is removed by the approximation

$$\sqrt{1 - \frac{2D}{B} \cos 2\psi} \approx 1 - \frac{D}{B} \cos 2\psi \quad (149)$$

Therefore

$$\mu_T = \frac{C_R}{(1+a)B(1 - \frac{D^2}{B^2})} (1 - \frac{D}{B} \cos 2\psi) \quad (150)$$

Equation (150) is in agreement with that given in reference 17. With the help of equations (139) and (141), whose friction terms have been neglected, and the relations

$$\epsilon_a = \frac{H_a}{H_R} \quad (151)$$

and

$$\epsilon_o = \frac{H_o}{H_R} \quad (152)$$

PRELIMINARY DATA

39

This material is not to be reproduced and is transmitted for the exclusive use of the indicated recipient. The data presented are tentative and subject to later revision or deletion. The opinions and conclusions expressed herein are those of the individual preparing this report and do not necessarily represent the views of the Naval Ordnance Test Station.

the reduced sensitivity may be rewritten in the form

$$\mu_T = \frac{C_R}{2kH_R^2 \cos^2 \theta_p (1+a)(2 + \epsilon_a^2 + \epsilon_e^2)} \left[\frac{1 - \left(\frac{\tan^2 \theta_p}{2} \right) \frac{(\epsilon_e^2 - \epsilon_a^2)}{(2 + \epsilon_a^2 + \epsilon_e^2)} \cos 2\psi}{1 - \left(\frac{\tan^2 \theta_p}{2} \right) \frac{(\epsilon_e^2 - \epsilon_a^2)^2}{(2 + \epsilon_a^2 + \epsilon_e^2)^2}} \right] \quad (153)$$

In the absence of trail currents the ideal sensitivity, analogous to equation (59), is

$$\mu = \frac{C_R}{4kH_R^2 \cos^2 \theta_p (1+a)} \quad (154)$$

The fractional reduction in sensitivity is

$$\frac{\mu - \mu_T}{\mu} = 1 - \frac{4 \left[2(2 + \epsilon_a^2 + \epsilon_e^2) - \tan^2 \theta_p (\epsilon_e^2 - \epsilon_a^2) \cos 2\psi \right]}{4(2 + \epsilon_a^2 + \epsilon_e^2)^2 - \tan^4 \theta_p (\epsilon_e^2 - \epsilon_a^2)^2} \quad (155)$$

Since the $\tan^4 \theta_p (\epsilon_e^2 - \epsilon_a^2)^2$ term may be neglected, equation (155) becomes

PRELIMINARY DATA

This material is not to be reproduced and is transmitted for the exclusive use of the indicated recipient. The data presented are tentative and subject to later revision or deletion. The opinions and conclusions expressed herein are those of the individual preparing this report and do not necessarily represent the views of the Naval Ordnance Test Station.

$$\frac{\mu - \mu_T}{\mu} = \frac{\epsilon_a^2 + \epsilon_e^2}{2 + \epsilon_a^2 + \epsilon_e^2} \left[1 + \frac{\tan^2 \theta_p (\epsilon_e^2 - \epsilon_a^2) \cos 2\psi}{(\epsilon_a^2 + \epsilon_e^2)(2 + \epsilon_a^2 + \epsilon_e^2)} \right] \quad *$$
(156)

Thus, in general, for a given pair of trail-to-range field ratios, ϵ_e and ϵ_a , the amount of reduction in sensitivity depends upon the direction ψ in which the kinematic lead is generated. In the special case in which the above ratios are equal, thus implying equal elevation and azimuth offsets, the amount of reduction is independent of the direction in which the kinematic lead is generated.

The above field ratios are directly proportional to the corresponding current ratios, and the constant of proportionality must depend on the numbers of turns in the coils as well as the coil form factors and permeability of the pole material. Thus

$$\left. \begin{aligned} \epsilon_e &= c_e \frac{I_e}{I_R} \\ \epsilon_a &= c_a \frac{I_a}{I_R} \end{aligned} \right\} \quad (157)$$

* It must be noted that equation (156) does not agree with equations (4) and (5) of reference 17 which gives as the corresponding expression

$$\frac{\mu - \mu_T}{\mu} = \frac{2(\epsilon_a^2 + \epsilon_e^2)}{2 + \epsilon_a^2 + \epsilon_e^2} \left[1 + \frac{0.48(\epsilon_e^2 - \epsilon_a^2)}{(\epsilon_a^2 + \epsilon_e^2)(2 + \epsilon_a^2 + \epsilon_e^2)} \right] \quad (156a)$$

where the \pm signs give the maximum and minimum values of reduction in sight sensitivity associated with $\psi = 0$ deg and $\psi = 90$ deg. Apparently 0.48 is $2 \tan^2 \theta_p$, where θ_p is 26 deg. At the date of this writing the present author has not been able to justify the above equation in preference to equation (156).

41

PRELIMINARY DATA

This material is not to be reproduced and is transmitted for the exclusive use of the indicated recipient. The data presented are tentative and subject to later revision or deletion. The opinions and conclusions expressed herein are those of the individual preparing this report and do not necessarily represent the views of the Naval Ordnance Test Station.

For some sight units the constants c_e and c_a are unequal due to the unequal numbers of turns on the elevation and azimuth trail coils. A slightly larger number of turns is provided on the azimuth coils than on the elevation coils to compensate for the smaller ratio of piper deflection to gyro axis deflection in azimuth than in elevation. This is done for the Sight Unit Mk 18. (See reference 7, Chapter 3, page 6.) Other sight units have equal numbers of turns on azimuth and elevation trail coils (i.e., $c_e = c_a$), and therefore slightly higher azimuth current than elevation current is required to obtain a given offset. The difference is introduced into the trail current mechanization constants in the associated computer. This is done for the modified Sight Unit Mk 8 (see reference 13).

When there are equal numbers of turns on azimuth and elevation trail coils, the reduction in sight sensitivity in terms of the currents becomes

$$\frac{\mu - \mu_T}{\mu} = \frac{c_a^2(I_a^2 + I_e^2)}{[2I_R^2 + c_a^2(I_a^2 + I_e^2)]} \left[1 + \frac{\tan^2 \theta_p I_R^2 (I_e^2 - I_a^2) \cos 2\psi}{(I_e^2 + I_a^2) [2I_R^2 + c_a^2(I_a^2 + I_e^2)]} \right] \quad (158)$$

A more useful form of the reduction of sensitivity would be in terms of the trail offset lead and the range current as is presented in reference 12, page 68*. The trail offset for a given I_e or I_a and I_R can be obtained approximately from equations (66) and (67) provided the ratio ϵ is small such that the hyperbolic dependence of trail offset on range current holds. However, for more accurate work the experimentally obtained curves of trail offset versus range current for different trail currents or their theoretical equivalent as developed in the section of these notes on actual trail offsets must be used.

Experimental curves, which were taken in order to determine the extent of the reduction of sensitivity by trail currents, are shown

* The present author has not been able to verify the table in reference 7 due to the lack of knowledge of the constants c_A or c_E relating field ratios to current ratios.

PRELIMINARY DATA

This material is not to be reproduced and is transmitted for the exclusive use of the indicated recipient. The data presented are tentative and subject to later revision or deletion. The opinions and conclusions expressed herein are those of the individual preparing this report and do not necessarily represent the views of the Naval Ordnance Test Station.

in Figure 18. However, the curves do not serve their intended purpose, since the true reduction due to trail currents as predicted by equation (158) is masked by the predominance of friction at the small angular deflections. The effect of friction is to make the reference sensitivity μ lower at the low angular rates than it is at the medium and higher angular rates. This is to be expected according to equation (77). For the lowest angular rates the sensitivity μ without trail currents is actually lower than the sensitivity μ_T with trail currents. To isolate the two effects more completely future studies should be made at higher angular rates where the effect of friction is negligible. The experimental data of Figure 18 were taken on a rate table with Sight Unit Mk 8 #311 modified according to reference 13, for $\psi = 90$ deg and $I_e = 0$ so that equation (158) takes on the special form of

$$\frac{\mu - \mu_T}{\mu} = \frac{c_a^2 I_a^2}{2I_R^2 + c_a^2 I_a^2} \left[1 + \frac{I_R^2 \tan^2 \theta_D}{2I_R^2 + c_a^2 I_a^2} \right] \quad (159)$$

From reference 18 for the Sight Unit Mk 18 Mod 0 the magnetic pole angle θ_D is 23.5 deg. It is assumed that the same angle is present in the Sight Unit Mk 8 #311 used in this experiment. From equations (44a) of reference 3, the constant c_a is 0.15. With these constants inserted in equation (159) the currents I_a and I_R are in milliamperes and are the appropriate values for the unmodified Sight Units Mk 8 as specified in reference 13. It is assumed that the same numbers of turns exist in the unmodified Sight Unit Mk 8 as in the Sight Unit Mk 18 Mod 0, for which the other constants θ_D and c_a are appropriate. According to reference 13 one may finally write the currents of equation (159) in terms of the currents I'_a and I'_R applied to the modified Sight Unit Mk 8 #311 used to obtain Figure 18 as

$$\begin{aligned} I_a &= 17.5 I'_a \\ I_R &= 4.26 I'_R \end{aligned} \quad (160)$$

The values of the trail offsets are obtained from the curves of trail offset versus range current for different I_e given in reference 12. A very rough spot check comparing the reduction as calculated from equation (159) and as obtained experimentally is given in the following table:

PRELIMINARY DATA

This material is not to be reproduced and is transmitted for the exclusive use of the indicated recipient. The data presented are tentative and subject to later revision or deletion. The opinions and conclusions expressed herein are those of the individual preparing this report and do not necessarily represent the views of the Naval Ordnance Test Station.

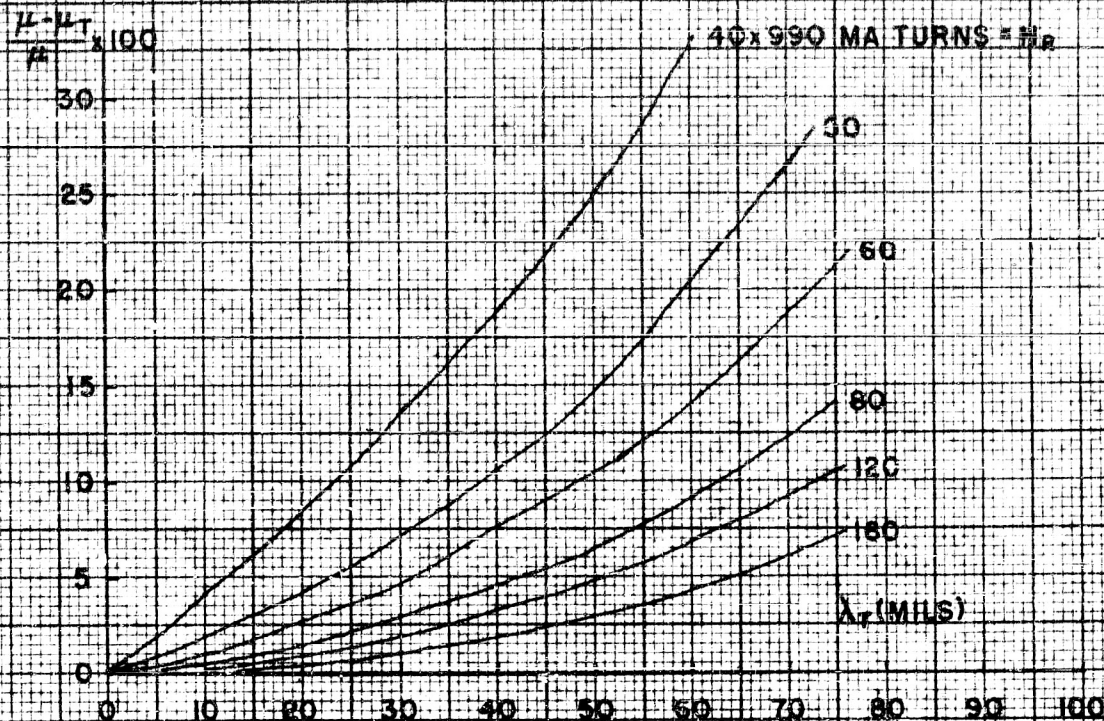


Figure 18(a) - Theoretical Plot of Average Reduction in Sight Sensitivity vs. Trail Offset (from table in ref. 12 p. 68)

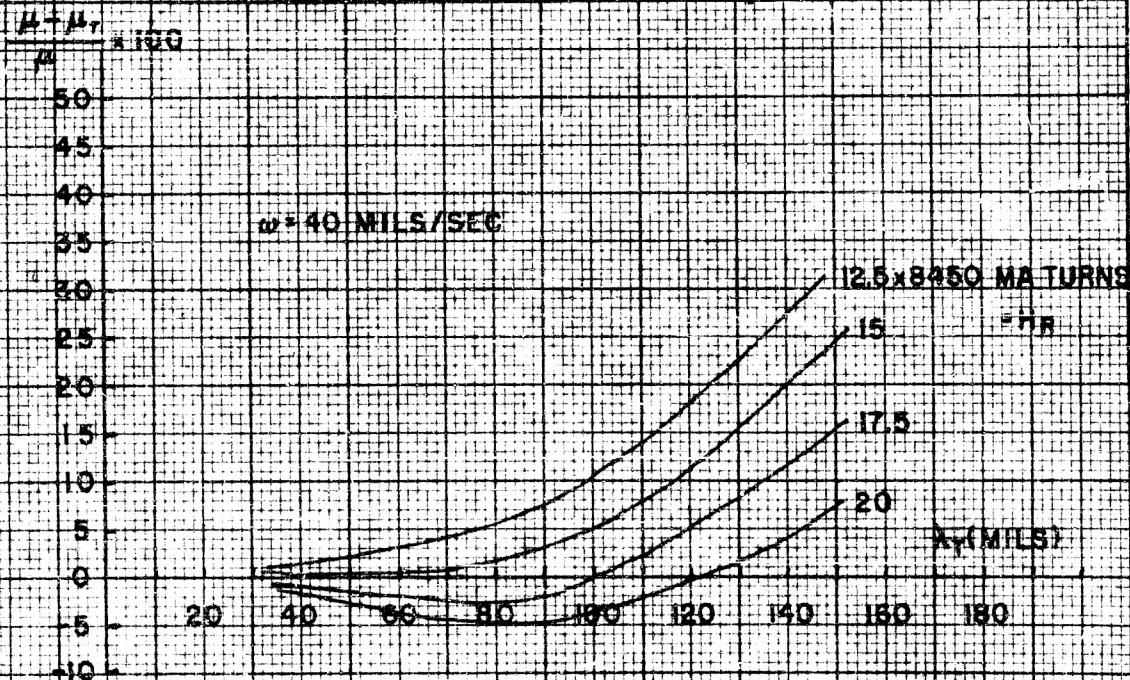


Figure 18(b) - Experimental Plot of Reduction of Sight Sensitivity in Elevation vs. Asimuth Trail Offset for $\omega = 40$ MILS/Sec. Reduction of reference sensitivity μ by friction accounts for apparent increase in sensitivity.

MADE IN U.S.A.
 12 1/2 x 10 1/2 x 10 1/2 IN. 100% COTTON FIBER
 100% COTTON FIBER

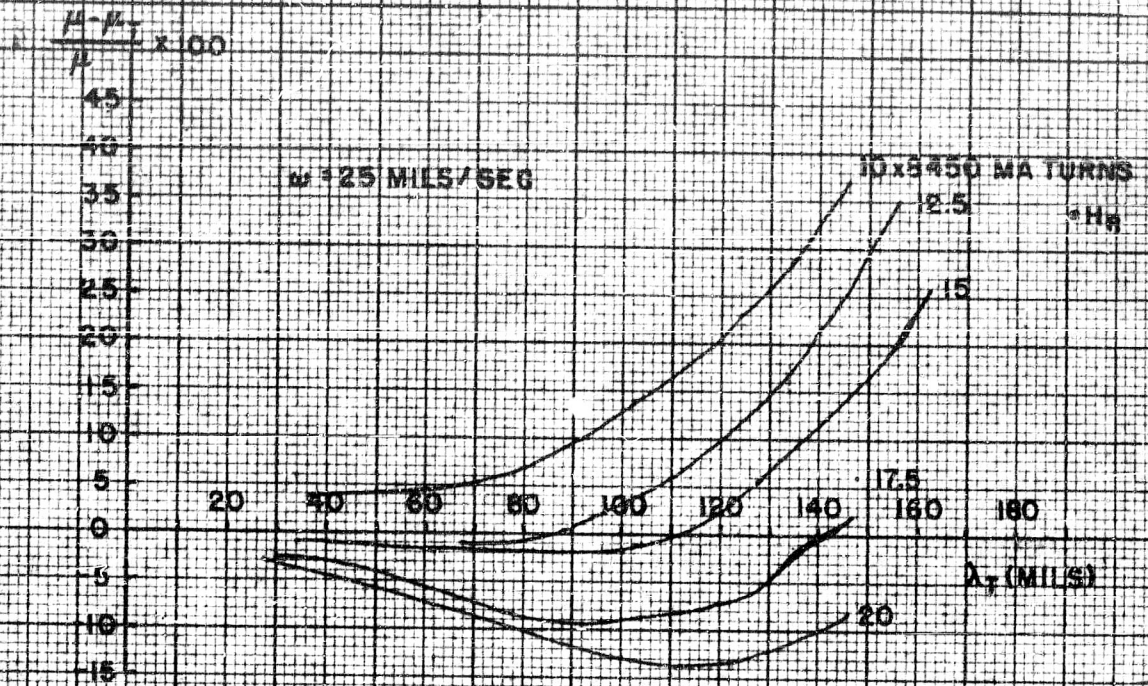


Figure 18(a) - Experimental Plot of Reduction of Sight Sensitivity in Elevation vs. Azimuth Trail Offsets for $\omega = 25$ mils/sec. Effect of friction is greater than in Figure 18(b)

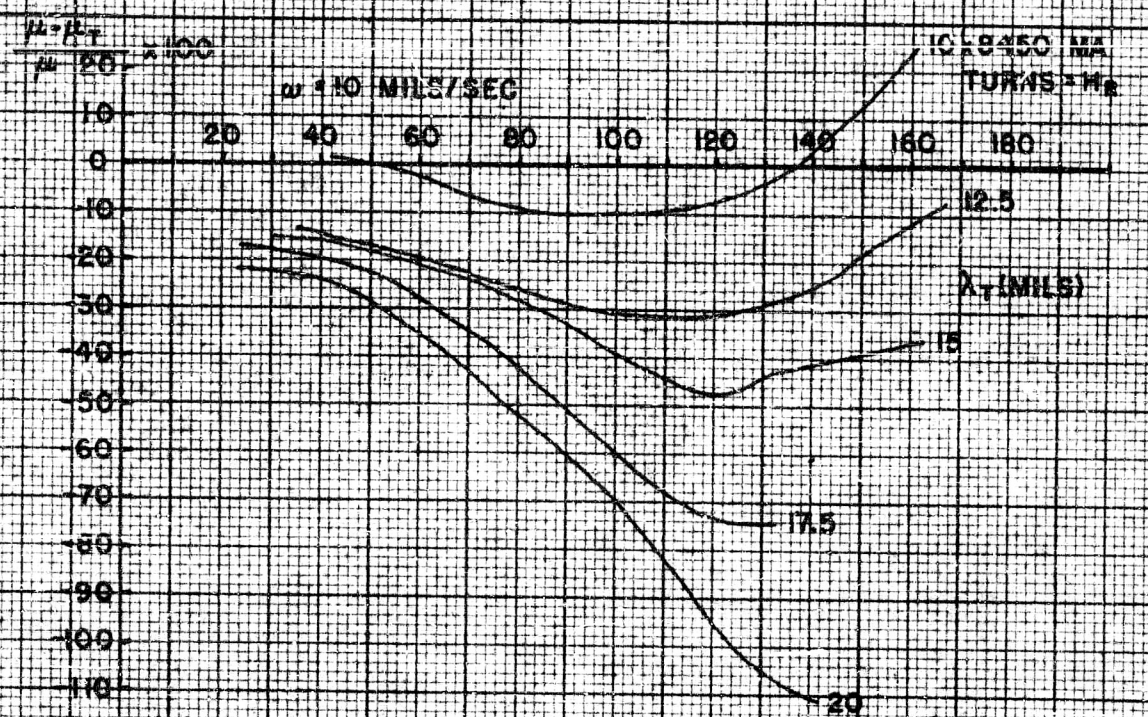


Figure 18(b) - Experimental Plot of Reduction of Sight Sensitivity in Elevation vs. Azimuth Trail Offset for $\omega = 10$ mils/sec. Friction

I_R (ma)	λ_a (mils)	Theoretical	Experimental
		$\frac{\mu - \mu_T}{\mu} \times 100$ (%)	$\frac{\mu - \mu_T}{\mu} \times 100$ (%)
30	100	5.7	5.3
30	140	16.3	20.0
25	120	10.0	18.2
25	146	17.9	32.5

The last two experimental values in the above table seem to be closer to the theoretical value determined from equation (156a) rather than from equation (156). However, if equation (156) is taken as the correct form in the absence of friction, then the increase in reduction of sensitivity over this value may possibly be accounted for by the friction terms present in equation (139) and described in reference 6. It is to be noted that the effect of friction on B of equation (139) and consequently on μ_T of equation (150) appears to be independent of angular rate and always produces a decrease in sight sensitivity. However, the effect of friction as described by equation (77) does depend on angular rate. A future more rigorous theory must give a more unified account of these effects. More comprehensive experiments to verify the above equations are being contemplated.

Resultant Sensitivity. Before an attempt is made to give an expression for the generalized sensitivity the sensitivities resulting from individual effects are reviewed.

The idealized sensitivity from equation (59) is

$$\mu = \frac{K^2}{(1 + a)I_R^2}$$

The above expression is not quite ideal due to the presence of the optical coupling constant which varies with direction of the kinematic lead. In the presence of an approximately constant pivot frictional

44

PRELIMINARY DATA

This material is not to be reproduced and is transmitted for the exclusive use of the indicated recipient. The data presented are tentative and subject to later revision or deletion. The opinions and conclusions expressed herein are those of the individual preparing this report and do not necessarily represent the views of the Naval Ordnance Test Station.

torque as described in equation (77) the sensitivity is

$$\mu_y = \mu \left(1 - \frac{2c_F}{\omega}\right)$$

Introducing the asymmetric air drag due to the proximity of the dome to the range coil retaining wall equation (87) gives approximately

$$\mu_A = \mu \left(1 + \frac{c_A}{I_R^2}\right)$$

Distortion of the eddy current pattern for large deflections gives the sensitivity the following form as obtained from equation (127).

$$\mu_E = \mu (1 + c_E \theta^2)$$

The temperature variation of the sensitivity is described by equation (132)

$$\mu_t = \mu_{40} \left[1 + 0.0032(t - 40)\right]$$

Finally the effect of trail currents for the special case of an azimuth kinematic lead and an azimuth offset in the same direction is given approximately by equation (136)

$$\mu_T = \frac{2\mu}{2 + c_B^2 \frac{I_B^2}{I_R^2}}$$

Although there is not too much value in writing down an expression for the generalized sensitivity, since the constants due to these effects are not well enough known, the following expression is suggested but should be considered only qualitatively:

PRELIMINARY DATA

This material is not to be reproduced and is transmitted for the exclusive use of the indicated recipient. The data presented are tentative and subject to later revision or deletion. The opinions and conclusions expressed herein are those of the individual preparing this report and do not necessarily represent the views of the Naval Ordnance Test Station.

$$\mu_{\text{gen}} = \frac{\mu_{40} \left[1 + 0.0032(t - 40) \right] \left(1 - \frac{c_R}{\omega} \right) \left(1 + \frac{c_A}{I_R} \right)}{m_1 \left(\frac{2 + m_2 \frac{I_a^2}{I_R^2}}{1 + m_3 \theta^2} - m_4 \right)} \quad (161)$$

where the m 's are constants.

OFFSETS OF AN ACTUAL SIGHT

The offsets of an actual sight obey the hyperbolic equation (67) as shown in Figure 11 only approximately. The agreement is best for moderate to high range currents. At low range currents the offsets decrease to zero as shown in Figure 19. A somewhat more accurate equation describing this effect is (61) which in terms of the currents reads

$$\lambda_a = 2k_a \frac{I_a}{I_R} \frac{1}{\left(2 + c_a^2 \frac{I_a^2}{I_R^2} \right)} \quad (162)$$

The maxima of these experimental curves of Figure 19 are seen to occur at higher range currents as the trail current increases. This fact is verified theoretically by setting the derivative of λ_a equal to zero and obtaining the range current for maximum offset as

$$(I_R)_c = I_a \sqrt{\frac{c_a}{2}} \quad (163)$$

The more general case when both elevation and azimuth offsets are present is described by equations (144). The offset terms are

PRELIMINARY DATA

This material is not to be reproduced and is transmitted for the exclusive use of the indicated recipient. The data presented are tentative and subject to later revision or deletion. The opinions and conclusions expressed herein are those of the individual preparing this report and do not necessarily represent the views of the Naval Ordnance Test Station.

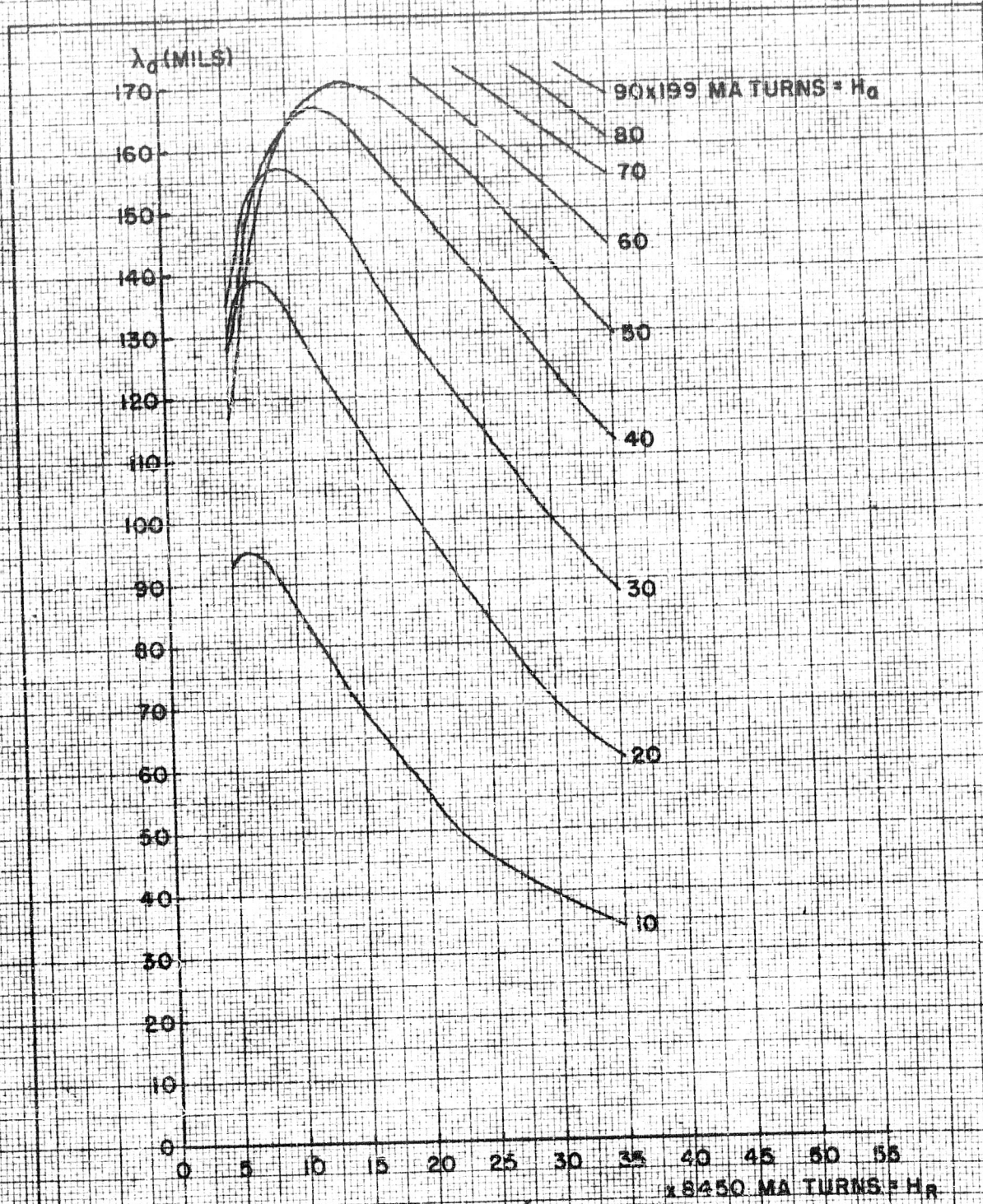


Figure 19
 Experimental Curves of Trail Offset (Azimuth) vs Range
 Field (or Current) for an Actual Sight. Similar Curve is
 obtained for the elevation offset.

$$\lambda_e = \frac{K_1(B + D)}{(1 + a)(B^2 - D^2 + C^2)} + \frac{K_2C}{(1 + a)(B^2 - D^2 + C^2)}$$

and

(164)

$$\lambda_a = \frac{K_1C}{(1 + a)(B^2 - D^2 + C^2)} - \frac{K_2(B - D)}{(1 + a)(B^2 - D^2 + C^2)}$$

After taking account of how K_1 , K_2 , B , and D are related to the magnetic fields H , H_e , and H_a through equations (139), (141), (142), and (143) it is apparent that the presence of one trail field alters the amount of offset due to the other trail field. The amount of this distortion for azimuth and elevation offsets up to 80 mils is shown in Figure 20 which was taken from references 10 and 12. For small azimuth offsets and large elevation offsets errors of the order of 5 mils are present. The errors are asymmetric and depend on the quadrant in which the resultant offset occurs. Referring to equation (164) it becomes apparent that if the Hooke's joint spider's moments of inertia and the Venturi torque were negligible (i.e., $C = 0$), there always results a reduction of one trail offset due to the presence of the other. However, actually C is not zero, and its effect is to add a term to the elevation offset whenever an azimuth offset is also present -- and similarly for the azimuth offset.

DIRECTION ERRORS IN THE PREDICTED LEAD

The classification of sight errors into two types, those of magnitude and those of direction, is perhaps, somewhat unsatisfactory, since most of the causes of one type of error are also responsible for the other type of error. For example, the variation of optical coupling between the gyro axis and sight line deflection with direction of deflection results in both an error in magnitude and direction of the predicted lead. Also pivot friction, Hooke's joint spider's moments of inertia, Venturi effect, large eddy currents, etc., all produce errors in both magnitude and direction. In the following sections the term "dip" applies to small deflections of the piper at right angles to the major or desired lead deflections.

47

PRELIMINARY DATA

This material is not to be reproduced and is transmitted for the exclusive use of the indicated recipient. The data presented are tentative and subject to later revision or deletion. The opinions and conclusions expressed herein are those of the individual preparing this report and do not necessarily represent the views of the Naval Ordnance Test Station.

H_0 - FIELD OF RANGE
 COILS - 250 X 990 MA
 TURBINE

SQUARE GRID GIVES DE
 FLECTIONS FOR IDEAL
 HYPERBOLIC RELATION

$$\frac{\Delta \theta}{\theta} = \frac{\Delta H}{H}$$

WHERE $\Delta \theta = 54$ MILS
 DISTORTED GRID GIVES
 EXPERIMENTAL DEFLEC
 TIONS WHICH THEREFORE
 MUST ALSO INCLUDE OR
 TICAL DIF AND LENS
 DISTORTION

ELEVATION DEFLECTION (MILS)

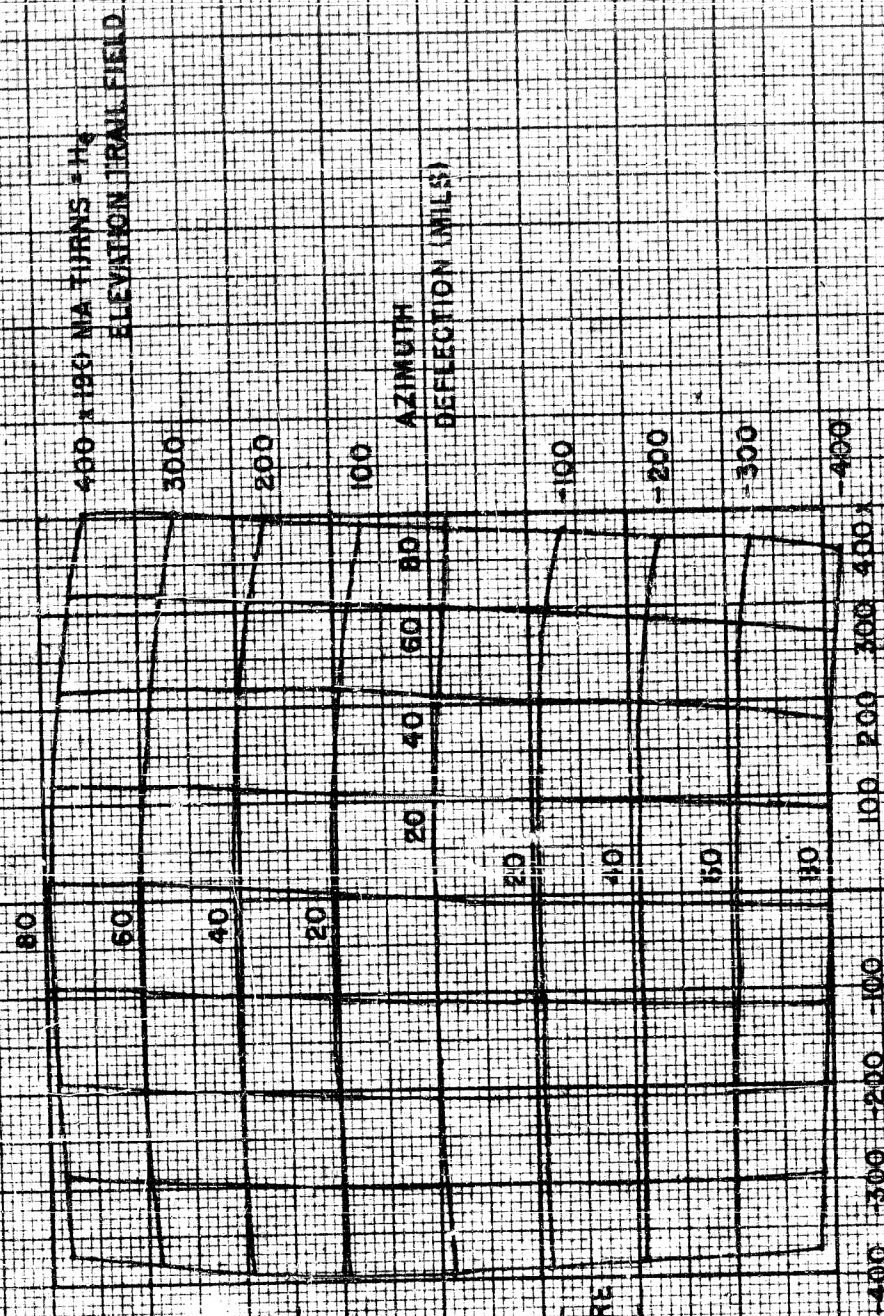


Figure 20

Distortion of Resultant Trail Offset in the Presence of Both Elevation
 and Azimuth Components (from reference 12)

OPTICAL DIP

When both azimuth and elevation components of deflection are present, the angular coordinates of the pipper are not given by the simple expressions for λ_A and λ_E of equations (40) and (41). The deflections may be shown to be interdependent according to the following relations:

$$\left. \begin{aligned} \lambda_A &= \frac{\cos \alpha}{1+a} \theta_A + \frac{\sin \alpha}{1+a} \theta_A \theta_E \\ \lambda_E &= \frac{1}{1+a} \theta_E - \frac{\sin \alpha \cos \alpha}{1+a} \theta_A^2 \end{aligned} \right\} (165)$$

For a derivation of equations (165) the reader is referred to reference 10.

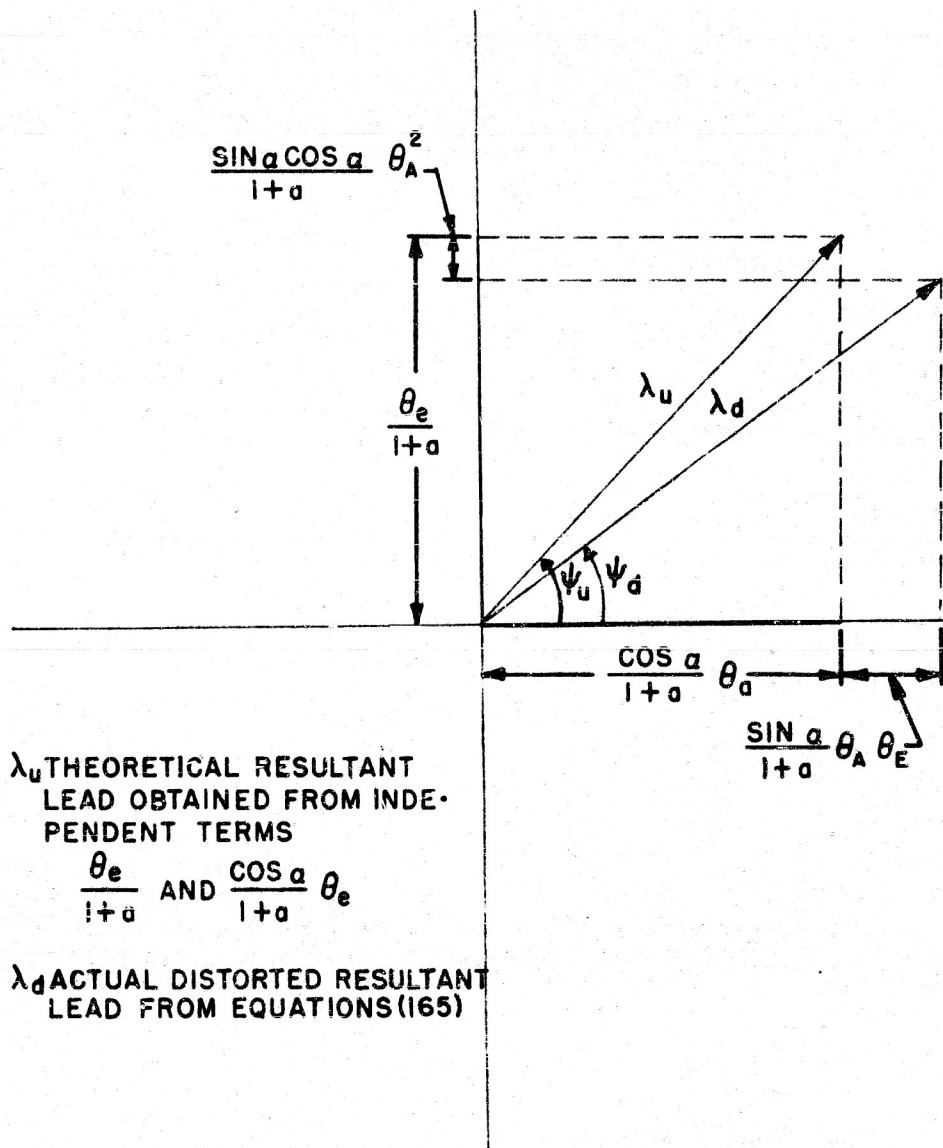
The effect of these additional terms is to distort the lead in both magnitude and direction as illustrated in Figures 21 and 22. As reported in reference 12 for the Sight Unit Mk 8 the maximum errors in magnitude are approximately 5 mils in elevation and 7 mils in azimuth and occur for the largest leads. By choosing calibration constants in the middle of the region of tactical interest as recommended in reference 11, these errors may be minimized.

LENS DISTORTION

The barrel distortion of the collimating lens is shown in Figure 23 as reproduced from reference 12. Maximum errors of 4 mils are present for large leads. In the region of downward leads near the vertical axis the optical dip error and the barrel distortion error partially compensate each other. For the new Sight Unit Mk 11 the optic axis of the collimating lens has been displaced 5 deg from the ADL ray, so that typical downward leads position the gyro reticle beam along the optic axis, thus minimizing the lens distortions. For more details on the internal geometry of the Sight Unit Mk 11 see reference 19.

PRELIMINARY DATA

This material is not to be reproduced and is transmitted for the exclusive use of the indicated recipient. The data presented are tentative and subject to later revision or deletion. The opinions and conclusions expressed herein are those of the individual preparing this report and do not necessarily represent the views of the Naval Ordnance Test Station.



λ_u THEORETICAL RESULTANT LEAD OBTAINED FROM INDEPENDENT TERMS

$$\frac{\theta_e}{1+a} \text{ AND } \frac{\cos a}{1+a} \theta_e$$

λ_d ACTUAL DISTORTED RESULTANT LEAD FROM EQUATIONS (165)

Figure 21
 Optical Dip Distortion of Resultant Lead
 in Presence of Both Azimuth and Elevation Components

350-11 KEUFFEL & ESSER CO.
10 X 10 to the 1/2 inch. 5th lines accented.
MADE IN U.S.A.



Figure 22
Optical Dip (from reference 12)

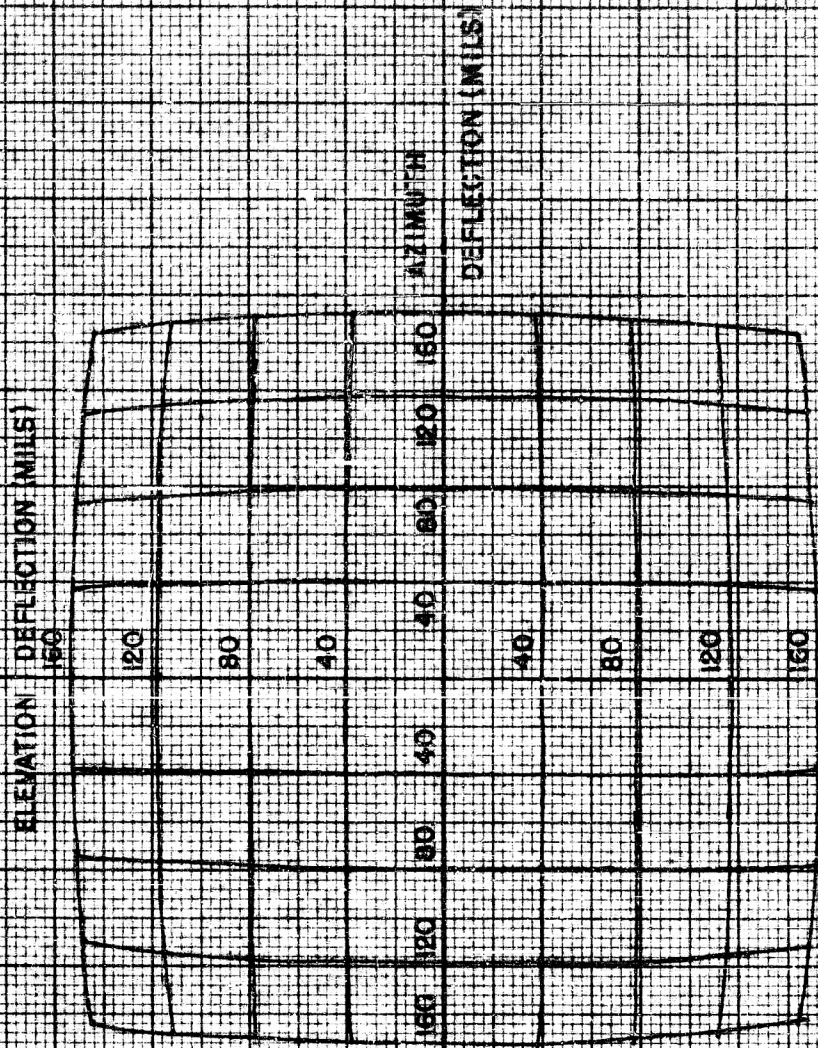


Figure 23

Lens Distortion (From reference 12)

MECHANICAL DIP

Mechanical dip is known to be caused chiefly by the finite moments of inertia of the Hooke's joint spider and a Venturi effect. Both effects produce torques and consequently angular momenta at right angles to the plane of the major deflection. The details of the torque due to spider inertia are developed in references 3, 6, 15, and especially 16.

The Venturi torque may be explained qualitatively as follows: when the spinning gyro mirror is tipped with respect to the case, in particular, with respect to the wall adjacent to the back side of the mirror, there is developed a high pressure-low velocity volume of air adjacent to a low pressure-high velocity volume of air at the mirror edge. According to Bernoulli's principle forces on the mirror will develop as shown in Figure 24. The resulting torque produces angular momentum perpendicular to the major deflection. Consequently a minor deflection of the gyro is produced at right angles to the major deflection.

Both the spider inertia and the Venturi effect are described analytically by the constant C as defined by equation (140) and used subsequently in equations (144), which are again

$$\lambda_E = \frac{-C_R(B + D)}{(1 + a)(B^2 - D^2 + C^2)} \omega_E + \frac{CC_R}{(1 + a)(B^2 - D^2 + C^2)} \omega_A$$

$$+ \frac{K_1(B + D)}{(1 + a)(B^2 - D^2 + C^2)} + \frac{K_2C}{(1 + a)(B^2 - D^2 + C^2)}$$

and

$$\lambda_A = \frac{-CC_R}{(1 + a)(B^2 - D^2 + C^2)} \omega_E - \frac{C_R(B - D)}{(1 + a)(B^2 - D^2 + C^2)} \omega_A$$

$$+ \frac{K_1C}{(1 + a)(B^2 - D^2 + C^2)} - \frac{K_2(B - D)}{(1 + a)(B^2 - D^2 + C^2)}$$

PRELIMINARY DATA

This material is not to be reproduced and is transmitted for the exclusive use of the indicated recipient. The data presented are tentative and subject to later revision or deletion. The opinions and conclusions expressed herein are those of the individual preparing this report and do not necessarily represent the views of the Naval Ordnance Test Station.

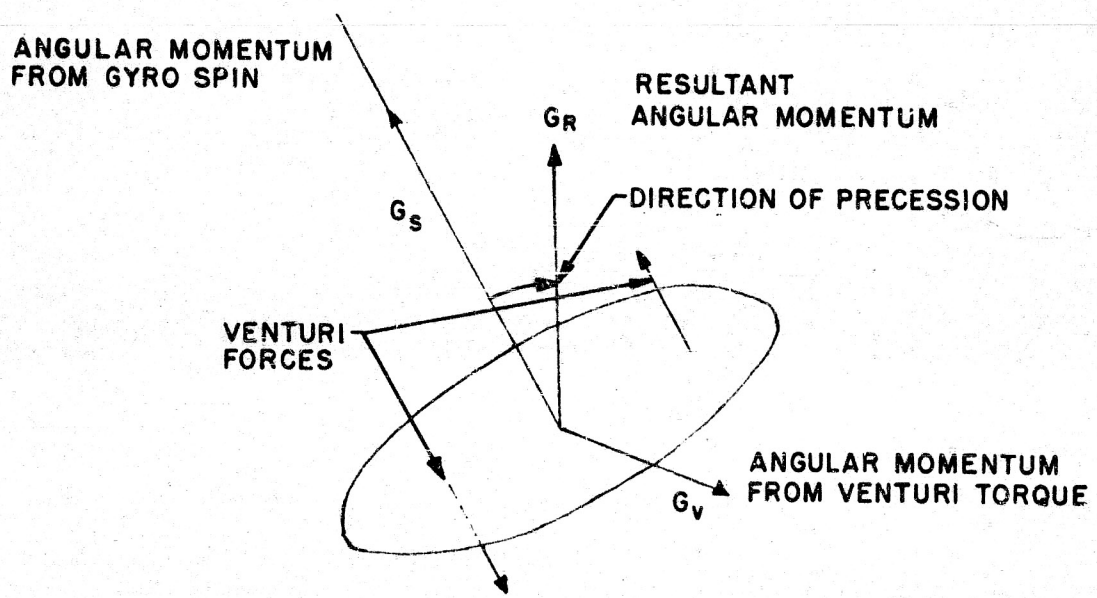
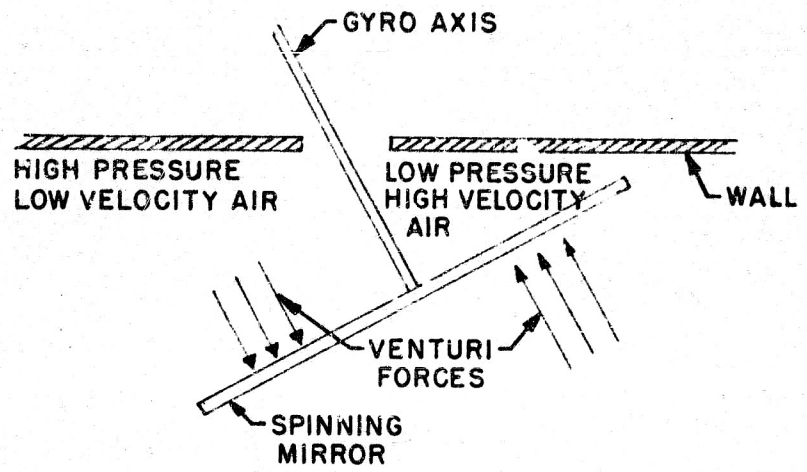


Figure 24
Mechanical Dip Distortion
Produced by the Venturi Torque

Since C is not zero, a rotation in the elevation (or azimuth) plane will produce an unwanted deflection in the azimuth (or elevation plane) as well as in the desired plane.

MAGNETIC DIP

Magnetic dip is due to the fact that the eddy current pattern is shifted in the direction of the rotating dome by a small amount. Thus the effective area in which the eddy current forces act is not directly under the poles but shifted as shown in Figure 25. The amount of shift of the eddy current pattern is given in terms of a time phase angle as

$$\phi = \tan^{-1} \delta v$$

from equation (119). The shifted eddy current pattern is described by equations (121). For the simple cosinusoidal field distribution extending over a distance b on the conducting sheet the actual distance d through which the current pattern is shifted is

$$d = \frac{2}{\pi} b \tag{166}$$

For small ϕ , $\phi = \delta v$ and therefore

$$d = \frac{\delta v b}{\pi} \tag{167}$$

or making use of equation (114)

$$d = \frac{2\sigma\mu vb^2}{\pi} \tag{168}$$

A measure of the displacement of the effective "magnetic" axes from the "geometric" axes is given by ψ_s which from Figure 25 is seen to be approximately

PRELIMINARY DATA

This material is not to be reproduced and is transmitted for the exclusive use of the indicated recipient. The data presented are tentative and subject to later revision or deletion. The opinions and conclusions expressed herein are those of the individual preparing this report and do not necessarily represent the views of the Naval Ordnance Test Station.

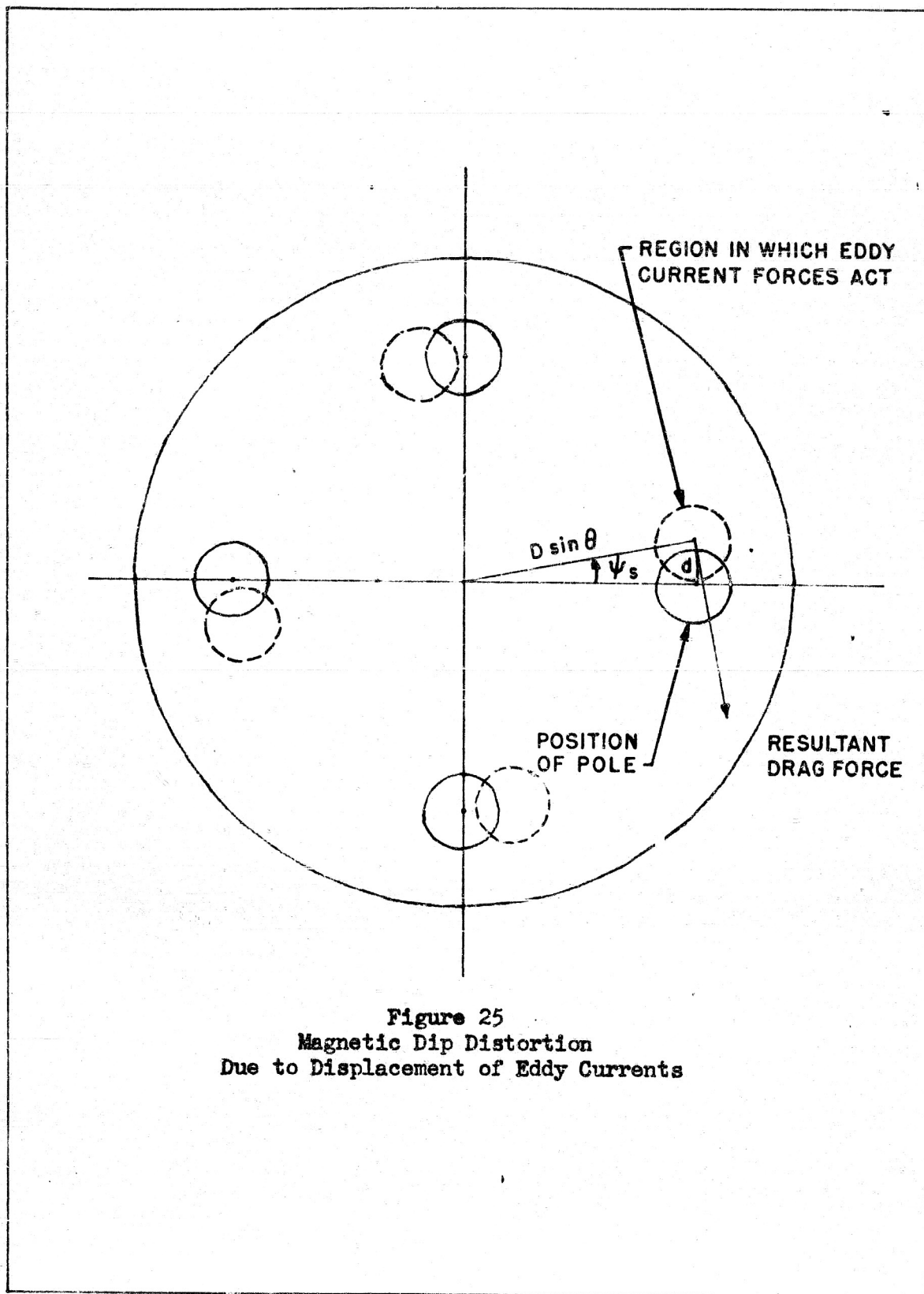


Figure 25
 Magnetic Dip Distortion
 Due to Displacement of Eddy Currents

$$\psi_s = \frac{d}{D \sin \theta} = \frac{2\sigma \mu v b^2}{w D \sin \theta}$$

Since $v = S D \sin \theta$ and μ is proportional to r/l

$$\psi_s = \text{const} \times \frac{\sigma r S A}{l} \quad (169)$$

where b^2 is proportional to the area A of the pole. The magnitude of ψ_s is of the order of one degree according to reference 5. The effect is independent of the gyro deflection θ but is proportional to the spin velocity S of the dome.

PRACTICAL ERROR ANALYSIS

The above sections on the theory of the errors of the sight head are given more to provide insight into the physical causes of the errors rather than to provide exact mathematical expression for the quantitative evaluation of the errors. Unfortunately too many of the constants, which are used in the above equations, have not been determined with sufficient accuracy to do the latter.

Detailed experimental curves, such as those of Figures 12 and 19, give the resultant gyro-predicted leads as composited from the many contributing causes, which were discussed in the preceding sections. Since the above theory is so complex and incomplete, it appears that the experimental data should be used whenever possible in assessing the errors of the sight.

Detailed methods of analysis and quantitative results of bias and random errors in the AFCS Mk 16 with particular emphasis on the errors of the sight head are the subjects of other memoranda which are still in preparation. Here, mention is merely made of three important types of sight head bias errors, which have been accounted for quantitatively in unpublished error analyses so far.

The first type of bias error is that due to the use of computer-mechanized constants, which are average values over the entire region of tactical use. In general, for almost any particular set

PRELIMINARY DATA

This material is not to be reproduced and is transmitted for the exclusive use of the indicated recipient. The data presented are tentative and subject to later revision or deletion. The opinions and conclusions expressed herein are those of the individual preparing this report and do not necessarily represent the views of the Naval Ordnance Test Station.

of tactical conditions, the experimentally determined values of K , k_e , and k_a are different from their average values. As reported in reference 13, the error in kinematic lead due to deviations of K from the average value, may be as high as 10 per cent in extreme cases but is usually much less. Errors in trail offset leads are of the same order of magnitude.

The second type of bias error is that due to the fact that the sight head when used with the AFCS Mk 16 is calibrated so that the gyro predicts less than the desired kinematic lead by the factor of $1/(1 + a)$. Other terms in the equation for the total lead are intended to partially compensate for this deficiency. The bias error results from lack of complete compensation. For the theory of this compensation the reader is referred to reference 4.

The third type of bias error is that due to reduction in sight sensitivity in the presence of trail offsets. No account has been taken of direction of kinematic lead relative to the direction of the resultant offset. Rather, average values of the reduction were used as given in references 10 and 12. These values may be too high in view of the apparent discrepancy between equations (156) and (156a).

IMPROVED SIGHTS

This section discusses sight improvements ranging from a minor change in factory calibration procedure of the present sight unit to rather major changes in design.

According to present factory calibration procedure as given in references 19 and 20 certain adjustments of the pole gap spacing are made so that the deflected pipper falls within the limits of a rectangular box on the calibration grid. The dimensions of this box are several mils on each side. It is felt that if in the future pipper deflections can be made to agree within one mil from one sight to the next, the sight dispersion especially with regard to the differences in k_e and k_a from sight to sight may be reduced considerably. The present dispersion for values of k_e and k_a as given in reference 13 is too large.

The Sight Unit Mk 11 is intended to be an improvement over the Sight Unit Mk 8. The gyro units are the same, but the optics of the Sight Unit Mk 11 have been improved. Greater eye and head

PRELIMINARY DATA

52

This material is not to be reproduced and is transmitted for the exclusive use of the indicated recipient. The data presented are tentative and subject to later revision or deletion. The opinions and conclusions expressed herein are those of the individual preparing this report and do not necessarily represent the views of the Naval Ordnance Test Station.

freedom are obtained by use of a single larger collimating lens, which transmits both gyro and fixed reticle beams to a much larger reflector plate. The sight no longer obstructs the pilot's view since it is installed forward of the instrument panel. By improved optical design the error due to optical coupling is halved. For more details on the Sight Unit Mk 11 the reader is referred to references 19, 21, 22, and 23.

In order to overcome the frictional effects which are most serious at low range currents and low angular rates, it has been proposed to increase the moment of inertia C_R of the gyro rotor about its axis of symmetry. However, according to reference 7, experiments with a heavier gyro revealed a greater amount of pivot friction due to the heavier load. Thus the kinematic lead response for low range currents was not improved. This effect may be noted in equations (144) wherein the friction terms F are contained in B . Thus B increased with C_R . However, the increased moment of inertia did result in reduction of dip for both the unwanted transverse components of the kinematic lead and of the fixed offsets. This shows up theoretically in equations (144), since the transverse lead is inversely proportional to the square of B instead of to the first power of B as in the desired components of lead. However, the over-all conclusion which was drawn from these experiments was that C_R should not be increased.

It has also been suggested that an air-driven gyro with a ball-bearing joint in place of the Hooke's joint might overcome the friction problem.

The magnetic distortion due to excessive reduction in restoring torque with large deflections might be lessened by making the second term in the denominator of equation (127)

$$T = \frac{k_1 \sigma AD^2 \mu^2 H^2 S \sin \theta}{1 + k_2 A \left(\frac{\sigma \tau DS}{b} \sin \theta \right)^2}$$

as small as possible but still maintain the required torque T . This might be done by lowering the conductivity σ of the dome by replacing aluminum by phosphor-bronze. The latter is also less sensitive to changes in temperature. To maintain the same torque the primary magnetic field H is raised. To avoid saturation difficulties such a

PRELIMINARY DATA

This material is not to be reproduced and is transmitted for the exclusive use of the indicated recipient. The data presented are tentative and subject to later revision or deletion. The opinions and conclusions expressed herein are those of the individual preparing this report and do not necessarily represent the views of the Naval Ordnance Test Station.

material as Permendur could be used. Lowering of the spin velocity S in the present eight units would necessitate sacrificing good gyroscopic properties. It is somewhat doubtful whether or not the dome thickness T could be reduced. However, if there is sufficient primary field H , then the pole gap spacing L could be increased and the pole area A decreased.

All the improvements mentioned above would also help reduce the magnetic dip as described by equation (169).

An inverted constraint system is described in reference 27 and consists of a moving magnetic pole fastened to a gyro and a fixed but slowly spinning dome fastened to the gyro housing. The magnetic pole is "focused" by the current in a range coil which surrounds the gyro housing. The magnetic path is also completed through the housing. Magnetic dip and friction are at a minimum but so far no satisfactory means of introducing trail offsets or pickup off information for the pilot have been devised.

JML/vms

Copy to

12

15

17

18

30

40

50

P80

35 (2)

3501

3502

3511

3512

3513

3521

3522 (Crockett)

3523

3524

5564 (3)

John M. Leffler
JOHN M. LEFFLER
Aviation Ordnance Department

On-Station Distribution Approved by

I. H. Swift
I. H. SWIFT, Head
Development Branch No. 1

54

PRELIMINARY DATA

This material is not to be reproduced and is transmitted for the exclusive use of the indicated recipient. The data presented are tentative and subject to later revision or deletion. The opinions and conclusions expressed herein are those of the individual preparing this report and do not necessarily represent the views of the Naval Ordnance Test Station.

BIBLIOGRAPHY

1. OP-1709 pt. 1, "Gunsight Mk 18 Mod 6, Description, Operation, Installation, Maintenance, Theory, Preservation, Packaging, and Storage" Bureau of Ordnance, dated 3 June 1948
2. LHC RTR #7, MMF 3-44-I, "Kinematics of the Hooke's Joint of the Gunsight Mk 18," by D.D. Cody, dated 11 March 1944
3. AMP Report 104.3R, "The Theory of an Electro-Magnetically Controlled Hooke's Joint Gyroscope," by D.P. Ling, dated October 1945
4. NOTS Technical Memorandum (in preparation) "Theory of AFCS Mk 16," by J. H. Cover
5. AMG-C #358, "Deflection Formulas for Gunsights of the Mk 18 Type," by D.P. Ling, dated 26 June 1945
6. LHC RTR #7, 1st supp. MFF 9-44-AA, "The Lead and Dip Computed by the Gyro in the Mk 18 Gunsight," by G.E. Albert, dated 21 September 1944
7. NOP RTR #22, "Characteristics of the Gun Sight Mk 23 with Increased Rotor Moment of Inertia," by P.L. Brink, dated 15 May 1947
8. LHC RTR #7, 1st supp. MFF-8-44-R, "Analysis of Optical Dip in the Gun Sight Mk 18," by N.J. Fine, dated 24 August 1944
9. AMG-C #261 (Working Paper), "Optical System of the Mk 18," by L.C. Hutchinson, dated 13 September 1944
10. NOPI RTR #23, "Summary Report on the Gunsight Mk 18 and Mods," by P.L. Brink and M. Cox, dated September 1947
11. NOTS Technical Memorandum #107, "Effect of Bank Angle on Optical Coupling and Predicted Kinematic Lead of a Gyroscopic Lead Computing Sight," by J. M. Leffler, dated 8 February 1951
12. NOPI RTR #24, "Aircraft Fire Control Systems Mks 5, 6, and 15, Air-to-Air Gunnery Calibration," by G.Y.T. Yu, dated June 1949
13. NOTS Technical Memorandum #111, "Calibration of the Sight Unit Mk 8 for Use with the AFCS Mk 16," by J. M. Leffler, W.F. Hassel, and R.R. Segel, dated 28 February 1951

PRELIMINARY DATA

55

This material is not to be reproduced and is transmitted for the exclusive use of the indicated recipient. The data presented are tentative and subject to later revision or deletion. The opinions and conclusions expressed herein are those of the individual preparing this report and do not necessarily represent the views of the Naval Ordnance Test Station.

BIBLIOGRAPHY (CONT)

14. NOP MFF 12-45-I, "G.S. Mk 23, Mod 1; Tests of Sight Heads with Modified Hooke's Joints," by F. Pleasonton, dated 28 December 1945
15. LHC RTR #7, MFF 7-4-44, "Analysis of the Torques on the Mk 18 Gunsight," by G.E. Albert, dated 4 July 1944
16. A.W.A. Paper No. 14, "The Theory of a Gyroscope Driven Through a Hooke's Coupling and Controlled by Eddy-Current Reaction," by L.B.C. Cunningham and M.S. Jones, dated November 1940
17. LHC RTR #7, 1st supp. MFF 8-44-M, "Variations in 'Time of Flight' For a Constant Range Current in the Mk 18 Gunsight," by G.E. Albert, dated 21 September 1944
18. Navy Department, Bureau of Ordnance, Dwg. No. 323512, "Gunsight Mk 18, Mod O, Gyro Housing Sub Assembly," dated 23 August 1945
19. NOTS Technical Memorandum #101, "Summary of Conference at Naval Ordnance Plant, Indianapolis, Regarding Sight Unit Mk 8," by J. M. Leffler, dated 23 January 1951
20. Gyro Calibration Card 9ND-NOP-2135 (formerly N-488(231)) (Rev. 7-49).
21. Memorandum to Re8 Files, "Notes on a Proposed New Sight," (Re8c)-SS:mhs, by S. Sparer, dated 1 February 1949
22. NOPI MFF 3-50-B, "Sight Unit Mk 11, Development of Experimental Model of," by E.B. Godley, 24 March 1950
23. Smythe, J.R., On Eddy Currents in a Rotating Disk, Electrical Engineering 61, 681-684, (September 1942)
24. Rudenberg, R., Energy of Eddy Currents in Electrical Brakes and Dynamomachines, Sammlung Elektrotechnische Vortrage, Verlag Enke, Stuttgart 1907. Bd 10 pp 269 and following
25. NOP MFF 3-49-B, app. B, "The Development of Equations which Account for the Electromagnetic Distortion of the Eddy-Current Torque," by P. Brink, dated 31 March 1949

PRELIMINARY DATA

This material is not to be reproduced and is transmitted for the exclusive use of the indicated recipient. The data presented are tentative and subject to later revision or deletion. The opinions and conclusions expressed herein are those of the individual preparing this report and do not necessarily represent the views of the Naval Ordnance Test Station.

BIBLIOGRAPHY (CONT)

26. NOTS Technical Memorandum (in preparation), "Magnetic Field Distribution in a Gyro Sight of the Mk 8 Type," by E.D. Simmons
27. NCP MMF 3-49-B, "Summary Report of the Status of the Development of an Eddy Current Constrained Gyroscope," by E.F. Echolds, dated 24 March 1949

PRELIMINARY DATA

This material is not to be reproduced and is transmitted for the exclusive use of the indicated recipient. The data presented are tentative and subject to later revision or deletion. The opinions and conclusions expressed herein are those of the individual preparing this report and do not necessarily represent the views of the Naval Ordnance Test Station.

AD-A800 076

22/7

STI-ATI-206 054

~~CONFIDENTIAL~~

251100

P19/5

Naval Ordnance Test Station, Inyokern, China Lake, Calif.

NOTES ON THE THEORY OF A GYROSCOPIC LEAD COMPUTING SIGHT OF THE MK 8 TYPE, by John M. Leffler. 17 May 51, 57p incl tables. Technical Memorandum 129.

NOTS-TM-129

DIV: Ordnance (22)

SECT: Fire Control & Bombing Systems (7)

SUBJECT HEADINGS

Gun sights, Computing

Gun sights, Gyroscopic

(Copies obtainable from ASTIA-DSC)

Target Lead

MICROFILMED

~~CONFIDENTIAL~~

CFSI RM NOTS Ser. 26 June 66